4-2016

Internal Fault Location in Transformer Windings

Samir Yehya Abed-Alkareem Alzekri
Western Michigan University

INTERNAL FAULT LOCATION IN TRANSFORMER WINDINGS

by

Samir Yehya Abed-Alkareem Alzekri

A thesis submitted to the Graduate College
in partial fulfillment of the requirements
for the degree of Master of Science in Engineering (Electrical)
Electrical and Computer Engineering
Western Michigan University
April 2016

Thesis Committee:

Pablo Gomez, Ph.D., Chair
Johnson Asumadu, Ph.D.
Ralph Tanner, Ph.D.

INTERNAL FAULT LOCATION IN TRANSFORMER WINDINGS

Samir Yehya Abed-Alkareem Alzekri, M.S.E.

Western Michigan University, 2016

Power transformers are one of the most important components in electrical power systems. During their lifetime they are exposed to various electrical faults which are originated from transient overvoltages, electromagnetic forces due to over-currents, ageing, etc.

Internal winding faults are among the most common causes of transformer failure. Once a fault occurs, a fast an efficient method for its detection and location is required to avoid further delays in the network operation. This paper introduces a simple method for the location of internal winding faults. This method is based on time domain terminal measurements of wave propagation along the winding. By means of low-cost laboratory components (a low-voltage DC source and an oscilloscope), different types of faults in layer–type windings can be detected and located with high accuracy. A frequency-domain distributed-parameter winding model is used to predict the transient response of the winding subjected to different types of faults. FEM simulations are used to compute the model parameters. A test case is presented to demonstrate the efficacy of the fault location method.

ACKNOWLEDGMENTS

I would like to express my sincere thanks for my advisor, Dr. Pablo Gomez, for his advice and support throughout this work. He introduced me to the world of research and encourage me to develop my own ideas for the problem while support me at each step with his knowledge and advice. Working with him has been a valuable experience for me and my continued education.

I would like to extend my thanks and appreciation to each member of my thesis committee, Dr. Johnson Asumadu, Ralph Tanner, for reviewing my thesis and their valuable suggestions. Lastly, my special thanks and gratitude go to my parents, my wife, and my friends for their supports and understanding while in graduate school.

Samir Yehya Abed-Alkareem Alzekri

TABLE OF CONTENTS

Table of Contents - Continued

CHAPTER

Table of Contents - Continued

CHAPTER

LIST OF FIGURES

List of Figures – Continued

List of Figures – Continued

CHAPTER 1

INTRODUCTION

The purpose of an electric power system is to provide electrical energy to all users in a reliable and continuous manner. The electricity consumption has increased in recent years because of the growth in population and the increased number of industries. This has increased the complexity and the size of electric power systems.

Most of the time the systems operate in a steady state. However, it is very important to study and analyze their behavior when a sudden change occurs. An electromagnetic transient is one of these conditions and is due to the interaction between electric energy stored in the capacitive elements and magnetic energy stored in the inductive elements of the system. As a consequence of this condition, power components are subjected to electric stresses which can result in operation failures [1].

Power transformers are one of the most important components in electrical power systems. During their lifetime they are exposed to various electrical faults which are originated from transient overvoltages, electromagnetic forces due to over-currents, ageing, among other causes [2].

According to the 2014 IEEE Report to the DOE Quadrennial Energy Review on Priority Issues, "25% of transmission infrastructure in the US is at an age where condition is a concern" [3]. Among this aging infrastructure, transformers are recognized among the

most important and costly power devices. From the different components of the transformer, between 30% and 50% of operating issues are related to winding damage [4] [5]. These issues often result in open or short circuit faults at specific turns along the windings. Once a fault occurs, a fast and an efficient method for its detection and localization is required to avoid further delays in the network operation.

1.1 Objectives

To present a simple and accurate time domain method for the detection and localization of internal faults in transformer windings, involving accessible and low-cost laboratory equipment.

1.2 Justification

Most of the fault location methods available to date rely on frequency response analysis (FRA) which, although very efficient, involves the application of highly specialized and costly equipment (frequency response analyzers, network analyzers or similar). Measurement setups using FRA can be time consuming and sensitive to the integrity of connections and possible source of EMI. Besides, interpreting the frequency response provided by these devices is a complicated task.

1.3 State of the Art

1.3.1 Transformer Models

In 1959, Rabins [6] introduced a new way to model a single layer transformer winding by considering it as a multiconductor transmission line.

In 1997, Shibuya et al. [7] used a frequency domain model based on single phase transmission line theory and multiconductor transmission line theory. They applied this model to a disc type transformer winding. The results were compared with measurements. Later, in 2001, Shibuya et al. [8] implemented a method to analyze high frequency transients in power transformer by reducing the number of unknowns when applying the multiconductor transmission line theory. The results were obtained using the fast Fourier transform (FFT) and compared with experiment measurements. The comparison confirmed the applicability of the method to the analysis of high frequency transients up to several megahertz. A frequency domain lumped parameter model was used in 2002 by Shibuya and Fujita [9] to analyze transient voltages in a transformer winding.

In 2001, Alfuhaid [10] presented a distributed parameter model in Laplace domain for frequency domain analysis of a single phase two-winding transformer. This model takes into account both the inductive and capacitive coupling between the two windings, and the inter-turn coupling within each winding. The results were compared with those obtained from the well-known circuit simulation program SPICE.

In 2006, Liang et al. [11] used a distributed parameter model based on multiconductor transmission line theory to determine the transfer function. Vector fitting and recursive convolution were used to obtain the response in time domain. The calculated results were validated using an experimental measurement.

In 2007, Popov et al. [12] presented a frequency domain model for a layer type transformer winding based on multiconductor transmission line theory. The iron core

losses and the proximity effect between layers were taken into account. The results were verified by experimental measurements, demonstrating that the model can be used to simulate the voltage distribution along the winding.

In 2008, Zhu et al. [13] presented a new hybrid model to simulate very fast transient overvoltages. The windings were divided into three sections. The first section was modeled based on multiconductor transmission line theory. A single phase transmission line was used to represent the second part of the winding, and the third section of the winding was modeled by equivalent lumped impedance. The results were validated with experimental measurements.

In 2014, Villanueva-Ramírez et al. [14] implemented two time domain transformer winding models for fast transient analysis using MATLAB/ Simulink. The first model is a lumped parameter model based on state-space equations, and the second model is based on multiconductor transmission line theory and Bergeron's method. Series losses were included in both models.

1.3.2 Parameters Determination for Transformer Model

In 1992, de Leon et al. [15] presented an efficient procedure for computing transformer parameters (turn leakage inductances and capacitances). The turns were used as a calculation base to allow modeling at very high frequencies. Turn-to-turn leakage inductances were obtained using the method of images. The capacitances between turns and turns to ground were calculated using the charge simulated method. This method was

validated by comparison with short circuit inductances computed with the finite element method and classical design formulas.

In 2005, Yan et al. [16] presented a method for inductance calculation of power transformers. This method is based on the transformer's magnetic circuit, and considers mutual and leakage inductances. The effect of vertical and horizontal leakage flux was considered. The results were compared with dynamic analog test.

In 2011, Li et al. [17] introduced a new method for computing the equivalent series capacitance and inductance of a unit coil for transient analysis of large transformers, using the FEM-based software Ansoft Maxwell. An electrostatic field solver and a 2D geometrical model were used for calculating the distributed capacitance of the winding, while a static magnetic field module and a 3D geometrical model were used to compute the inductance.

Also in 2011, Gomez et al. [18] presented a technique to compute the inductance matrix of transformer windings for a very fast transients. This technique is based on the application of a multilayer method of images, and is able to take the effect of the core into consideration when computing the inductance matrix. The results were compared with an electromagnetic field simulation using FEM, and showed an excellent accuracy. In 2013, Gomez et al. [19] introduced an improvement to the previous method for calculating the inductance matrix of multilayer windings.

In 2012, Eslamian et al. [20] used a new analytical method for computing the inductance matrix for transformer winding at high frequencies. The effect of the core was taken into considered. The inductance outside the core was computed by a numerical integration of the potential vector. The core was replaced by an image source with the correct magnitude and location. Two different methods based on an analytical solution of the Poisson equation in planar coordinates were used to calculate the inductance inside the core window. In both methods, the inductances were computed by applying the magnetic energy method.

1.3.3 Fault Detection Methods

In 2001, De et al. [21] proposed a method for fault detection in power transformers involving an artificial neural network as a pattern recognition technique to recognize the frequency response of the winding admittance of a typical high voltage transformer under healthy and different faulty conditions of winding insulation. A lumped parameter high frequency model of the winding, based on a coil-by-coil representation of the windings, was used and developed using EMTP. Discrete fast Fourier transformation (DFFT) was used to convert the amplitude time data into the corresponding amplitude frequency spectrum of the waves in form of vectors.

In 2004, Zhang et al. [25] proposed a method for insulation fault detection of power transformers using the genetic programming (GP) method. The proposed method was implemented using database of actual gas records from transformers. This database consists of 352 gas records and their actual fault type diagnosed by experts. Only five fault

types were included in this database (no fault, medium temperature thermal, high temperature thermal, low energy discharge, and high energy). Four genetic programming classifiers (GPC) were generated by GPQUICK software to classify the five types of faults.

In 2007, Nandi [22] proposed a technique to detect the inter-turn faults by utilizing the saturation effects of the transformer core. The sensitivity even for one turn fault is very high. However, it requires to compare with information for the healthy transformer. This method was verified using both simulation and experiments on a bank of three single phase transformers.

In 2007, Yadaiah et al. [23] presented a methodology for off-line and on-line fault detection in power transformers. An artificial neural network was used to detect off-line faults and a discrete wavelet transforms to detect on-line faults. An artificial neural network method based on dissolved gas analysis was used to overcome the limitations of existing methods. The discrete wavelet transform for on-line fault detection involves measurement of the current signal at the primary terminal of the power transformer and determines the detail and approximate coefficients of discrete wavelet transform. These coefficients characterize the condition of the system.

In 2014, Mahvi et al. [2] presented a new technique for sensitive detection and localization of shorted turns on the windings. Using genetic algorithm, the detailed model of the damaged winding by the fault is estimated from the measured low frequency response data up to 10 kHz. The fault is localized along the winding by comparing between the healthy and faulty transfer functions of the winding using statistical indicators. This

method was tested on transformer damaged by a low level short circuit fault. The results showed that this method is sufficiently able to detect and localize failures due to shorted turns on the transformer windings.

In 2015, Aljohani et al. [24] presented a way to identify the minimum level of a short circuit fault within power transformers that can be detected using frequency response analysis (FRA) technique. The model used in this paper is a physical geometrical arrangement of a three phase transformer, using three dimensional finite element analysis to simulate its physical operational conditions. Short circuit faults at different levels were simulated, comparing the faulty response from the FRA with the healthy response. The results showed that there is a minimum detection level of a short circuit fault that can be detected using FRA technique. Results showed that short circuit fault levels higher than 5% can be identified using the FRA technique.

1.4 Contributions

- An alternative time domain method for fault detection in layer type transformer winding is proposed.
- Unlike existing fault location techniques, the proposed method requires only low cost, readily available and easy to use equipment: a low voltage DC source and an oscilloscope with two channels.
- A flow chart, based on extensive simulations on a distributed parameter model defined in the frequency domain, was produced as a guide to apply the proposed method.

1.5 Limitations and Scope

1.5.1 Limitations

- The proposed time domain method for fault detection in transformer winding is restricted to layer type transformers. Further tests are required to extend the method to other winding configurations.
- The method is able to detect three types of faults:
    1. Short circuit between neighboring turns
    2. Short circuit between neighboring layers
    3. Open circuit
- The results have not been validated experimentally. However, the model used to test the fault location method has been previously validated by other authors.

1.5.2 Scope

- The transformer winding model used to define and test the proposed method is a distributed parameter model defined in the frequency domain. This model was implemented using MATLAB.
- Regarding the computation of electrical parameters required by the transformer winding model: the capacitance matrix was obtained using the commercial software COMSOL Multiphysics (based on the finite element method), while the inductance matrix and losses were computed using analytical formulas.

- The accuracy of the fault location method was assessed considering a 303-turns layer type transformer winding model and applying different types of faults at diverse locations along the winding.

1.6 Thesis Outline

Chapter 1, Introduction: This chapter includes introduction, objectives, justification, limitations, and contributions of this thesis. In addition, the state of art on the subject is presented.

Chapter 2, Transformer Winding Modeling for Fast Transient Analysis: The model applied for the development and testing of the proposed fault detection method is described in this chapter. A comparison between the lumped and distributed parameter models is also included, as well as a discussion of the advantages of using a distributed parameter model.

Chapter 3, Parameter Determination for High-Frequency Electromagnetic Transients: Several methods for calculating the parameters of high frequency transformer model are described in this chapter. Furthermore, a case study for computing the parameters of a transformer winding using commercial software COMSOL Multiphysics is introduced.

Chapter 4, Internal Fault Analysis and Location: The proposed method for fault detection and location in transformer windings is introduced in this chapter. Also, the simulation results for different type of faults at different locations and the ability of the method to diagnose and localize the fault is demonstrated.

Chapter 5, Conclusion and Future Work: The main results and achievements of this thesis are summarized, indicating possible future work.

CHAPTER 2

TRANSFORMER WINDING MODELING FOR FAST TRANSIENT ANALYSIS

2.1 Introduction

An electromagnetic transient is a sudden change in a circuit condition due to the interaction between electric energy stored in the capacitive elements and magnetic energy stored in the inductive elements. This phenomenon can occur in a power component or system as a consequence of a switching operation, a lightning event or a fault condition. After transmission lines, power transformers are the elements of the system with the highest exposure to electromagnetic transients [26]. These phenomena can be classified, according to the frequency content of the resulting surges, in low to mid-frequency transients (slow-front surges), and high-frequency transients (fast-front surges). The type of excitation applied for the fault detection method described in this thesis corresponds to the latter classification. Therefore, the remaining of this Chapter describes the modeling approach for high-frequency transients, also known as fast transients. Studying this phenomenon by means of modeling and simulation tools usually requires the implementation of very detailed models of the transformer winding considering a turn-by-turn representation which includes inductive, capacitive and loss components [26]. Figure 2.1 shows a typical representation of a segment of a transformer winding [27], where L is the series inductance of the winding, R is its series resistance, Cs is the capacitance between turns, Rs is the loss component of Cs, Cg is the capacitance to ground, and Rg is the loss

component of Cg. Based on this circuit. Starting from this circuit, the most common modeling approaches are based on applying circuit theory (lumped parameter models) or transmission line theory (distributed parameter models). The models described in this section are both defined in the frequency domain in order to consider the frequency dependence of the winding parameters in a direct manner. The distributed parameter model is based on a multiconductor transmission line representation and zig-zag connection to preserve the continuity between conductors (turns) [28]. The lumped parameter model is based on the nodal definition of a system consisting of *N* segments defined according to Fig. 1.

When the length of each turn of the winding is far less than the wavelength, a turn can be represented by a lumped element (lumped parameter model). This modeling approach does not take into account the wave traveling along each turn. Therefore, it can be inaccurate when the pulse applied has a very short rise time. This problem can be overcome by using a distributed parameter model [29].

Taking into account the wave propagation along the winding allows a more accurate transient analysis. This feature makes the distributed parameter model a better candidate than the lumped parameter one for the fault detection method described in this thesis.

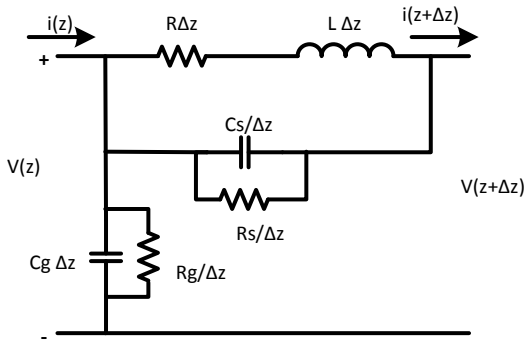

Figure 2.1 Equivalent circuit per unit length of the winding of a transformer [27]

2.2 Distributed Parameter Model

The ability to properly consider wave propagation along the winding and the frequency dependence of the winding parameters are the most important advantages of using a distributed parameter model defined in the frequency domain. For that reason, it is considered as the most accurate model currently available [30]. In this model, each conductor of a multiconductor transmission line model represents a turn of the winding. The end of each conductor and the beginning of next conductor are connected to simulate the continuity between turns of the winding [14].

2.2.1 Telegrapher Equations of Multiconductor Transmission Line

The telegrapher equations define the wave propagation along a transmission line. They are defined in the time domain as [27]

$$-\frac{\partial \mathbf{v}(z,t)}{\partial z} = \mathbf{R}\,\mathbf{i}(z,t) + \mathbf{L}\frac{\partial \mathbf{i}(z,t)}{\partial t} \tag{2.1}$$

$$-\frac{\partial \mathbf{i}(z,t)}{\partial z} = \mathbf{G}\,\mathbf{v}(z,t) + \mathbf{C}\frac{\partial \mathbf{v}(z,t)}{\partial t} \tag{2.2}$$

where $\mathbf{v}(z,t)$ and $\mathbf{i}(z,t)$ are the voltage and current waves, R and L are the matrices of series resistance and inductance.

Applying the Laplace transform to obtain the corresponding equations in the frequency domain:

$$-\frac{d\mathbf{V}(z,s)}{dz} = \mathbf{R}\,\mathbf{I}(z,s) + s\mathbf{L}\mathbf{I}(z,s) \tag{2.3}$$

$$-\frac{d\mathbf{I}(z,s)}{dz} = \mathbf{G}\,\mathbf{V}(z,s) + s\mathbf{C}\mathbf{V}(z,s) \tag{2.4}$$

One of the advantages of using frequency domain analysis is the simplicity of finding the solution for the system since the original partial differential equations (2.1) and (2.2) are transformed into the ordinary differential equations (2.3) and (2.4). In addition, it is substantially easier to include the frequency dependence of the winding parameters if the equations are defined in the frequency domain [28], [31]. In contrast, defining frequency dependent parameters in time domain would require solving convolution operations.

The time domain result will be obtained using the numerical Inverse Laplace Transform as describe in Appendix B.

2.2.2 General Solution For The Telegrapher Equations in The Frequency Domain

Defining:

$$V(z,s) = V$$

$$I(z,s) = I$$

$$Z = R + sL$$

$$Y = G + sC$$

Taking the second derivative of (2.3) and (2.4) and combining the results:

$$-\frac{d^2\boldsymbol{V}}{dz} = \boldsymbol{ZYV} \tag{2.5}$$

$$-\frac{d^2\mathbf{I}}{dz} = \boldsymbol{YZI} \tag{2.6}$$

where **Z** and **Y** are matrices of size *n*x*n* (*n* = number of conductors or turns), and **V** and **I** are column vectors of length *n*.

Applying modal decomposition, the general solution of equation (2.5) is given by

$$\boldsymbol{V} = \exp(-\boldsymbol{\Psi}_z)\ \boldsymbol{C}_1 + \ \exp(+\boldsymbol{\Psi}_z)\ \boldsymbol{C}_2 \tag{2.7}$$

where

$$\boldsymbol{\Psi} = \boldsymbol{M}\sqrt{\boldsymbol{\lambda}}\boldsymbol{M}^{-1} \tag{2.8}$$

M and **λ** are the matrices of eigenvectors and eigenvalues of the **ZY** product, respectively. The general solution for the current is obtained using the first telegrapher equation in the frequency domain and solving for the current:

$$\boldsymbol{I} = -\boldsymbol{Z}^{-1}\frac{d\boldsymbol{V}}{dz} \tag{2.9}$$

Substituting (2.7) in (2.9):

$$\boldsymbol{I} = \boldsymbol{Y}_o[\exp(-\boldsymbol{\Psi} z)\ \boldsymbol{C}_1 - \exp(+\boldsymbol{\Psi} z)\ \ \boldsymbol{C}_2] \tag{2.10}$$

where

$$\boldsymbol{Y}_o = \boldsymbol{Z}^{-1}\boldsymbol{\Psi} \tag{2.11}$$

2.2.2 Two-Port Nodal Form

Starting from the general solution for the voltages and currents and applying boundary conditions, the following admittance matrix form is obtained, which relates voltages and currents at both ends of the line [32], [28]:

$$\begin{bmatrix} \boldsymbol{I}_o(s) \\ \boldsymbol{I}_l(s) \end{bmatrix} = \begin{bmatrix} \boldsymbol{Y}_{ss} & -\boldsymbol{Y}_{sr} \\ -\boldsymbol{Y}_{rs} & \boldsymbol{Y}_{rr} \end{bmatrix} \begin{bmatrix} \boldsymbol{V}_o(s) \\ \boldsymbol{V}_l(s) \end{bmatrix} \tag{2.12}$$

Equation (2.12) can be represented by the equivalent Π-circuit shown in Fig. 2.2. This model can be used for transformer winding modeling by adding a zig-zag connection, as shown in Figure 2.3. The admittances required to perform this connection modify (2.12) as follows:

$$\begin{bmatrix} \mathbf{I}_0(s) \\ \mathbf{I}_L(s) \end{bmatrix} = \begin{bmatrix} \boldsymbol{Y}_{ss} + \mathbf{Y}_{con11} & -(\boldsymbol{Y}_{sr} + \mathbf{Y}_{con12}) \\ -(\boldsymbol{Y}_{rs} + \mathbf{Y}_{con21}) & \boldsymbol{Y}_{rr} + \mathbf{Y}_{con22} \end{bmatrix} \begin{bmatrix} \mathbf{V}_0(s) \\ \mathbf{V}_L(s) \end{bmatrix} \tag{2.13}$$

where

$$\mathbf{Y}_{con11} = \begin{bmatrix} \mathrm{Y}_S & 0 & \cdots & 0 & 0 \\ 0 & \mathrm{Y}_{con} & \cdots & 0 & 0 \\ \vdots & \vdots & \ddots & \vdots & \vdots \\ 0 & 0 & \cdots & \mathrm{Y}_{con} & 0 \\ 0 & 0 & \cdots & 0 & \mathrm{Y}_{con} \end{bmatrix} \tag{2.14}$$

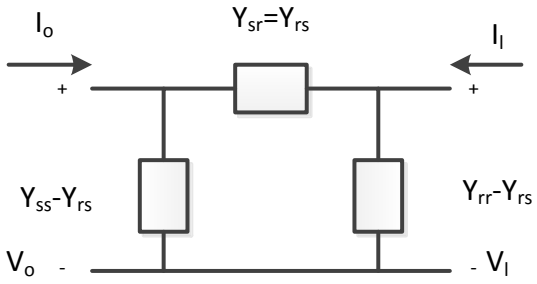

Figure 2.2 Admittance model for multiconductor transmission line [28]

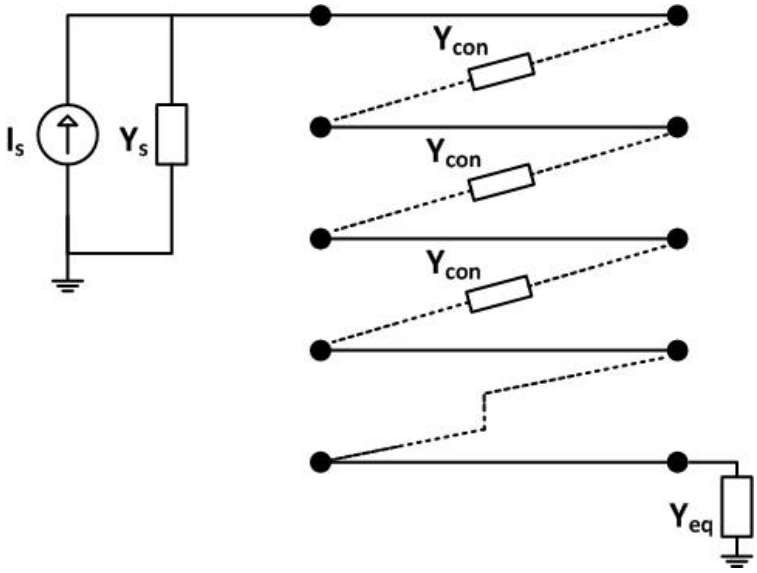

Figure 2.3 MTL model of transformer winding [14]

$$\mathbf{Y}_{con21} = \begin{bmatrix} 0 & Y_{con} & \cdots & 0 & 0 \\ \vdots & \vdots & \ddots & \vdots & \vdots \\ 0 & 0 & \cdots & Y_{con} & 0 \\ 0 & 0 & \cdots & 0 & Y_{con} \\ 0 & 0 & \cdots & 0 & 0 \end{bmatrix} \tag{2.15}$$

$$\mathbf{Y}_{con22} = \begin{bmatrix} Y_{con} & 0 & \cdots & 0 & 0 \\ 0 & Y_{con} & \cdots & 0 & 0 \\ \vdots & \vdots & \ddots & \vdots & \vdots \\ 0 & 0 & \cdots & Y_{con} & 0 \\ 0 & 0 & \cdots & 0 & Y_{eq} \end{bmatrix} \quad (2.16)$$

In equations (2.14) to (2.16), Y_{con} is a large admittance used to simulate the zig-zag connection, and Y_{eq} is the admittance connected at the end of the winding. The source shown in Figure 2.3 is defined in terms of a Norton equivalent, where Y_S is the Norton's admittance and I_s is the Norton's injection current.

2.3 Lumped Parameter Model

One of the disadvantages of the distributed parameter model is the large computer time required. A lumped parameter model can be an alternative when the detailed representation of every turn in the winding is not required. This model is based on a circuit network obtained by a cascaded connection of *n* segments (turns), each represented by the circuit shown in Figure 2.1 [30], [33]. This is illustrated in Figure 2.4.

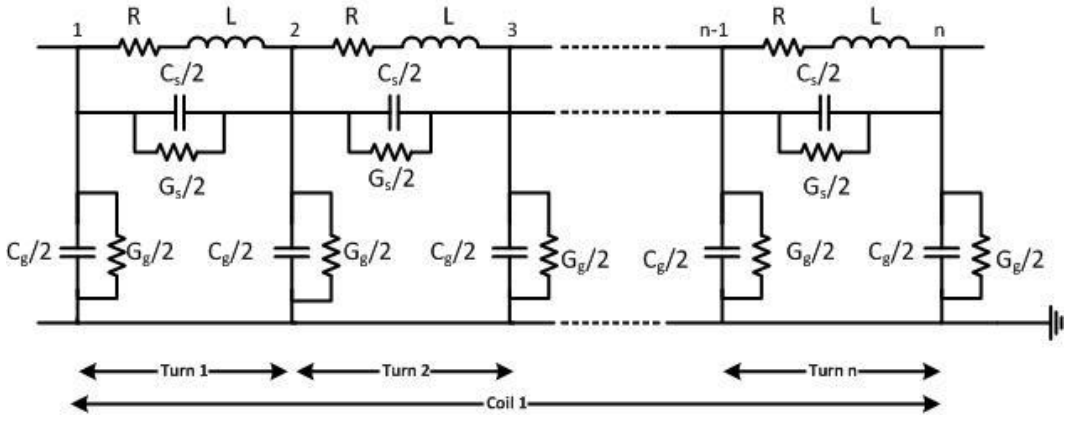

Figure 2.4 Equivalent circuit of transformer winding including losses [30]

2.3.1 Model Based on State Equation Without Series Losses

Application of nodal analysis to the circuit shown in Figure 2.4 results in

$$s\hat{\mathbf{C}}\hat{\mathbf{V}}(s) + \hat{\mathbf{G}}\hat{\mathbf{V}}(s) + \frac{\hat{\mathbf{\Gamma}}}{s}\hat{\mathbf{V}}(s) = 0 \tag{2.17}$$

where

$\hat{\mathbf{C}}$ = nodal capacitance matrix with the inclusion of input node

$\hat{\mathbf{G}}$ = nodal conductance matrix with the inclusion of input node

$\hat{\mathbf{\Gamma}}$ = nodal matrix of inverse inductances with the inclusion of input node

$\hat{\mathbf{V}}(s)$ = output vector of node voltages with the inclusion of input node

The number of the equations is reduced by extracting the input node *k* because its voltage is known. This results in the following equation [28] [32]:

$$s\mathbf{C}\mathbf{V}(s) + \mathbf{G}\mathbf{V}(s) + \frac{\mathbf{\Gamma}}{s}\mathbf{V}(s) = -s\mathbf{C}_k U(s) - \mathbf{G}_k U(s) - \frac{\mathbf{\Gamma}_k}{s}U(s) \tag{2.18}$$

where

C = nodal capacitance matrix without the input node

G = nodal conductance matrix without the input node

Γ = nodal matrix of inverse inductance without the input node

V(*s*) = output vector of node voltages without the input node

U(*s*) = known voltage of the input node

$\mathbf{C}_k$, $\mathbf{G}_k$ and $\mathbf{\Gamma}_k$ = *k*-th columns of **C**, **G** and **Γ** with row *k* removed.

Rewriting (2.18) in compact form, an admittance model is defined:

$$\mathbf{I}(s) = \mathbf{Y}(s)\mathbf{V}(s) \tag{2.19}$$

where **Y**(*s*) is the nodal admittance matrix of the circuit, and **I**(*s*) is the nodal current vector, given by

$$\boldsymbol{Y}(s) = s\boldsymbol{C} + \boldsymbol{G} + \frac{\mathbf{\Gamma}}{s} \tag{2.20}$$

$$\boldsymbol{I}(s) = -s\boldsymbol{C}_k\boldsymbol{U}(s) - \boldsymbol{G}_k\boldsymbol{U}(s) - \frac{\mathbf{\Gamma}_k}{s}\boldsymbol{U}(s) \tag{2.21}$$

CHAPTER 3

PARAMETER DETERMINATION FOR HIGH-FREQUENCY ELECTROMAGNETIC TRANSIENTS

This chapter describes existing methods for the calculation of electrical parameters of transformer windings for high-frequency transients. It also explains an alternative parameter calculation based on the finite element method (FEM) by means of commercial software COMSOL Multiphysics.

3.1 Introduction

Inductive, capacitive and losses components are very important for the correct description of the behavior of transformer windings for fast transient studies. Regardless of the model used to analyze the voltage distribution along the winding, these parameters must be described correctly at high frequencies. Parameter calculation can be developed using simplified analytical expressions, laboratory tests, or an electromagnetic simulation tool, such as COMSOL Multiphysics [27].

The flux penetration into the core is usually neglected for very fast transients, especially for the first few microseconds [34], considering that the core acts as a magnetic insulation wall at high frequencies, The core inductance is considered to behave as a completely linear element since high-frequency yields reduced magnetic flux density [27].

3.2 Calculation of the Capacitance Matrix

Capacitance is defined as the ratio of a potential difference between two conductors and the electric charge stored between them [35].

To make a correct estimate of the voltage distribution along a transformer winding under the effect of a high-frequency transient phenomenon, it is necessary to obtain the values of series capacitance and capacitance to ground [32].

3.2.1 Analytical Expressions

The most common way to compute the winding capacitances is based on the formula for parallel plates [27]:

$$C = \frac{\varepsilon_o \varepsilon_r A}{d} \tag{3.1}$$

where:

ε_o is the free space permittivity

ε_r is the relative permittivity of the dielectric material between turn

A is the plate area

d_s is the distance between plates

Figure 3.1 shows the representation of two discs of a transformer winding, including the different types of capacitances present in this arrangement [27].

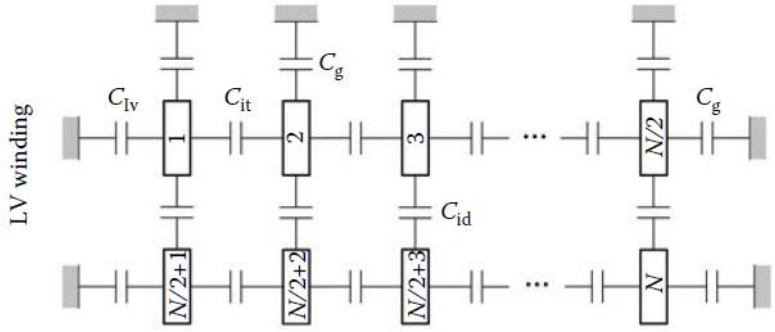

Figure 3.1 Representation of two discs of transformer winding [27].

In Figure 3.1:

C_{lv} is the capacitance between the HV and LV sides.

C_{it} is the capacitance between turns.

C_g is the capacitance between turn and ground.

C_{id} is the capacitance between discs.

Computing these four types of capacitances is done applying equation (3.1), considering the dielectric permittivity, distance between elements, and transversal area for each element:

$$C_{it} = \frac{\varepsilon_o \varepsilon_r \, h}{d_{IT}} \tag{3.2}$$

$$C_{id} = \frac{\varepsilon_o \varepsilon_r \, w}{d_{ID}} \tag{3.3}$$

$$C_{lv} = \frac{\varepsilon_o \varepsilon_r \, h}{d_{LV}} \tag{3.4}$$

$$C_g = \frac{\varepsilon_o \varepsilon_r \, w}{d_G} \tag{3.5}$$

where

w is the conductor's width

h is the conductor's height

d_{IT} is the distance between turns

d_{ID} is the distance between discs

d_{LV} is the distance between HV side and LV side

d_g is the distance between turn and ground plane

The parallel plate formula for computing the capacitance assumes that he electric field is always straight and perpendicular to the plates. In practice, electric field behavior near the edges of the plates is different. This phenomenon is known as fringe effect. The following modified formulas take into account this effect in the calculation of capacitances between turns and between disks [5]:

$$C_{it} = \frac{\varepsilon_o \varepsilon_{it} (w + d_{it})}{d_{it}} \tag{3.6}$$

$$C_{id} = \varepsilon_o \left(\frac{k}{{d_{it}}/{\varepsilon_{it}} + {d_{id}}/{\varepsilon_{oil}}} + \frac{1-k}{{d_{it}}/{\varepsilon_{it}} + {d_{id}}/{\varepsilon_{id}}} \right) (R + d_{id}) \tag{3.7}$$

where

ε_{it} and ε_{id} are the relative permittivity of the insulation between turns and between discs

ε_{oil} is relative permittivity of the oil insulation

$d_{it}\ and\ d_{id}$ are the distances between turn and between discs

K is the fraction of circumferential space occupied by oil

R is the winding's radial depth

3.2.2 Finite Element Method

A more general and accurate capacitance calculation can be obtained from an electrostatic field simulation. The most common approaches based on finite element method (FEM) to evaluate the elements of the winding capacitance matrix are [27]:

- Forced voltage
- Fixed charge
- Energy method

Forced Voltage

For simplicity, only 4 elements are considered. The following system is defined:

$$\begin{bmatrix} Q_1 \\ Q_2 \\ Q_3 \\ Q_4 \end{bmatrix} = \begin{bmatrix} C_{11} & C_{12} & C_{13} & C_{14} \\ C_{21} & C_{22} & C_{23} & C_{24} \\ C_{31} & C_{32} & C_{33} & C_{34} \\ C_{41} & C_{42} & C_{43} & C_{44} \end{bmatrix} \begin{bmatrix} V_1 \\ V_2 \\ V_3 \\ V_4 \end{bmatrix} \tag{3.8}$$

The first step is to excite one of the turns. Electric charges from all four elements are computed using FEM. Applying voltage to turn i, elements $C_{1i},\ C_{2i},\ C_{3i}, C_{4i}$ (column i) from the capacitance matrix shown in (3.8) are obtained. The complete capacitance matrix is obtained after four simulations. In general, the number of simulations needed to obtain the complete capacitance matrix is equal to the number of turns in the winding.

Fixed Charge

This method is used when the charges are known, and voltages are unknown. In this case, the values obtained are the elements of the inverse of the capacitance, as follows:

$$\begin{bmatrix} V_1 \\ V_2 \\ V_3 \\ V_4 \end{bmatrix} = \begin{bmatrix} C_{11} & C_{12} & C_{13} & C_{14} \\ C_{21} & C_{22} & C_{23} & C_{24} \\ C_{31} & C_{32} & C_{33} & C_{34} \\ C_{41} & C_{42} & C_{43} & C_{44} \end{bmatrix}^{-1} \begin{bmatrix} Q_1 \\ Q_2 \\ Q_3 \\ Q_4 \end{bmatrix} \tag{3.9}$$

Energy Method

In this method, the self-capacitance C_{ii} of the winding is computed from the electrostatic energy when applying a voltage V_i to the turn i, according to the following equation:

$$C_{ii} = \frac{2W_{ei}}{V_i^2} \tag{3.10}$$

Mutual capacitance C_{ij} is computed from the energy obtained when applying voltage to turns i and j, as follows:

$$C_{ij} = \frac{W_{eij} - \frac{1}{2}\left(C_{ii}V_i^2 + C_{jj}V_j^2\right)}{V_i V_j} \tag{3.11}$$

where

W_{ei} is the electrostatic energy due to exciting the turn i

W_{eij} is the electrostatic energy due to exciting both i and j turns

3.3 Calculation of the Inductance Matrix

To calculate the inductance in a winding with an iron core for fast transient analysis, it is usually assumed that the magnetic flux is concentrated in the air space due to the fact that the time required for the magnetic flux to penetrate to the ferromagnetic material is greater than the duration of the transient period. Therefore, it is common to replace the iron core with an air core for transient analysis. However, it has been shown recently that this assumption introduces a significant error in the calculation due to eddy currents. Iron core behaves as a barrier against the magnetic flux at high frequencies, which is not the same as considering an air core [18].

3.3.1 Analytical Expressions

Before the computer age, several authors proposed different analytical formulas to calculate the self and the mutual inductance of coil arrangements. One of these traditional

formulas was defined by Maxwell as an exact expression for the mutual inductance between two thin wire rings (negligible transversal area, as shown in Figure (3.2) [36]:

$$L_{AB} = \mu_o \sqrt{R_1 R_2} \left[\left(1 - \frac{k^2}{2} \right) K(k) - E(k) \right] \tag{3.12}$$

where

$$k = \sqrt{\frac{4R_1 R_2}{(R_1 + R_1)^2 + d^2}} \tag{3.13}$$

K (*k*) and *E* (*k*) are the first and second order elliptical integrals, respectively. μ_o is the permeability of vacuum.

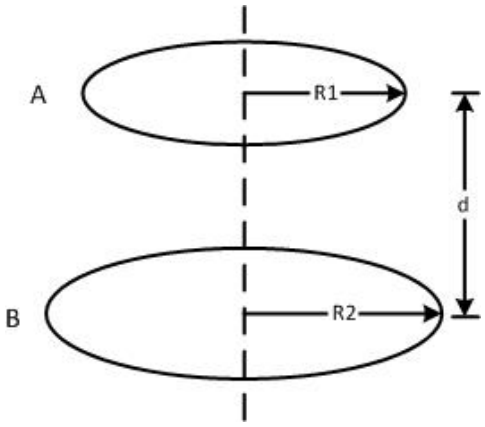

Figure 3.2 Mutual inductance between two thin wires [36]

3.3.2 Finite Element Method

There are two main approaches for the computation of self and mutual inductances applying the finite element method:

1. Method of flux linkage
2. Method of energy

Method of Flux Linkage

Magnetic flux Ψ across a surface *s* is considered in this method, as shown in Figure (3.3). This results in the following expressions:

$$\Psi = \iint \mathbf{B} \cdot d\mathbf{s} \tag{3.14}$$

$$L = \frac{\Psi}{i} \tag{3.15}$$

where:

Ψ is the total magnetic flux

B is the magnetic flux density

i is the current in the conductor

L is the corresponding inductance

To calculate the mutual inductance L_{ij}, conductor i is excited and i^{th} flux that cross the surface of conductor j is integrated, as shown in Figure 3.4.

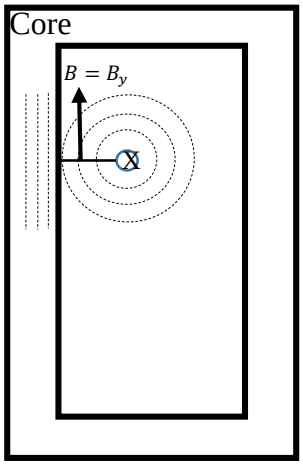

Figure 3.3 Computing the self-inductance using the flux linkage method [28]

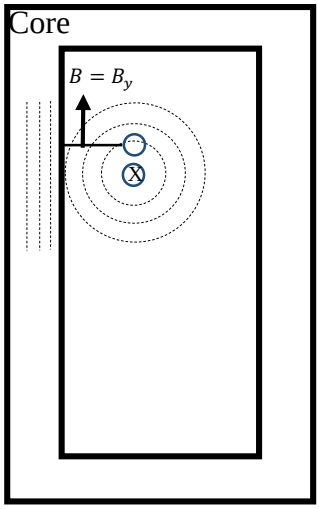

Figure 3.4 Computing the mutual inductance using the flux linkage method [28]

Method of Energy

Similar to the calculation of the capacitance matrix, the inductance matrix can be computed using the magnetic energy. For computing the self-inductance, conductor *i* is excited with current I_i and the following expression is applied:

$$L_{ii} = \frac{2W_{mag,i}}{I_i^2} \tag{3.16}$$

Mutual inductance $L_{ij}$is computed from the energy obtained when exciting turns *i* and *j*, as follows:

$$L_{ij} = \frac{W_{mag,ij} - \frac{1}{2}\left(L_{ii}I_i^2 + L_{jj}I_j^2\right)}{I_i I_j} \tag{3.17}$$

According to (3.17), all self-elements need to be computed before computing the mutual elements.

3.4 Calculation of Loss Components

At steady state, losses are undesirable and costly for physical systems. However, for high-frequency transients in transformer windings they have a positive effect in reducing the magnitudes of transient oscillations. Transformer losses result from many sources, each one with different characteristics [1].

The losses caused by the current flowing in transformer winding conductors has three components: direct current (dc) losses, skin effect losses and proximity effect losses.

Taking into account the dc losses and skin effect at high frequency and considering a rectangular cross section, the impedance of the conductor per unit length is calculated as [27]:

$$Z_c = \sqrt{R_{dc}^2 + Z_{hf}^2} \tag{3.18}$$

$$R_{dc} = \frac{\rho_c}{A} \tag{3.19}$$

$$Z_{hf} = \frac{\rho_c}{2p(w+h)} \tag{3.20}$$

where

ρ_c is the resistivity of the conductor

A is the cross-sectional area of the conductor

p is the penetration depth, defined as

$$p = \sqrt{\frac{\rho_c}{j\omega\mu_o}} \tag{3.21}$$

An alternative way to consider both skin and proximity effects is by the following relationship [37], [34]:

$$\mathbf{R} = \frac{1}{d}\sqrt{\frac{2\omega}{\sigma_c\mu_c}}\mathbf{L} \tag{3.22}$$

So the impedance matrix will be

$$\mathbf{Z} = \mathbf{R} + j\omega\mathbf{L} \tag{3.23}$$

3.5 Case Study

A layer type transformer winding is considered. It contains 303 turns in three layers (101 turns per layer), as shown in Figure 3.5. The capacitance matrix is obtained using the fixed voltage method, through the electrostatic module of COMSOL Multiphysics 5.1.

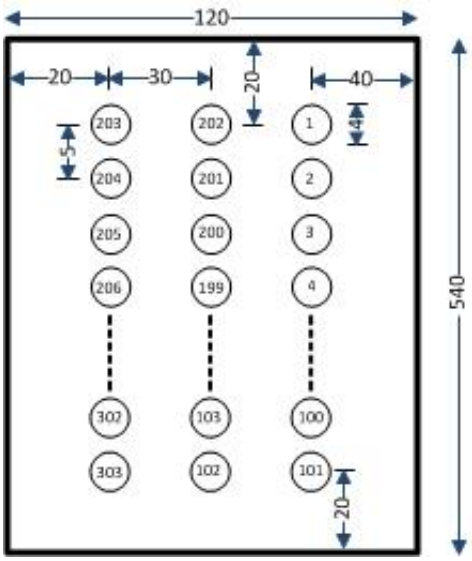

Figure 3.5 Turns connection for three layer transformer

The actual geometrical arrangement of the winding is 3-dimensional. However, a good approximation can be achieved by means of a 2-dimensional simplification considering the existing geometrical symmetries. The cross section of the winding is constructed in a 2-D geometry inside the core window [38] [39].

One of the most important aspects of the finite element method is the meshing size. Smaller mesh elements are considered close to the conductors to get better results, as shown in Figure 3.6.

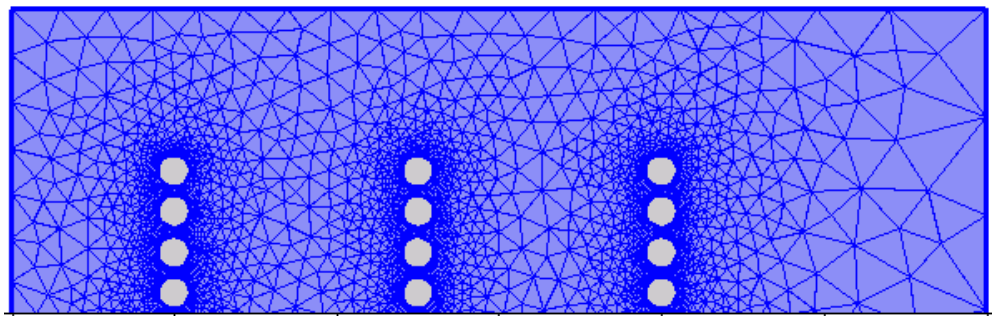

Figure 3.6 Meshing for calculation of the capacitance matrix

One of the methods used in COMSOL to compute the capacitance is called fixed voltage, as described in Section 3.2.2. COMSOL provides the user with a very useful feature to perform this task, called terminal. A terminal number is specified for each turn, and one of the turns is defined as excited by means of a voltage. COMSOL computes the self-capacitance for that turn and the mutual capacitances with that turn. In other words, a column vector is obtained.

To compute the whole capacitance matrix of size 303x303, 303 simulations are required (one simulation for each column). In order to make this set of simulations easier, COMSOL has another useful feature called parametric sweep. Using this feature, *n* simulations can be performed in a single step. For each simulation, the turn to be excited will change from 1 to 303.

For the test case, the inductance matrix of the winding was obtained directly from the capacitance matrix according to the following relationship [34]:

$$\mathbf{L} = \mu_o \varepsilon_o \mathbf{C}^{-1} \tag{3.24}$$

Finally, the skin and proximity effects were taken into account by means of (3.24). The result for this test case is shown in Appendix A.

CHAPTER 4

INTERNAL FAULT ANALYSIS AND LOCATION

4.1 Introduction

Transformers are recognized among the most important and costly components of the power grid. From the different transformer elements, a large percentage of operating issues occur in the windings. This often results in open or short circuit faults between specific turns [5]. Once a fault condition occurs, an efficient and accurate method is required for its detection and location in order to avoid further delays in the network operation.

Most of the methods available to date for fault detection in transformer windings are based on frequency response analysis (FRA). This method can be very accurate, but it also requires highly specialized and costly equipment (frequency response analyzers, network analyzers or similar). Fault location methods relying on frequency response analysis can be time-consuming and sensitive to electromagnetic noise. Also, interpreting the results from FRA is a complicated task which can only be completed by a highly qualified person.

4.2 Fault Detection Method

An alternative time domain method for fault detection in transformer windings is introduced in this chapter. The only equipment required are a low voltage DC source and

an oscilloscope with two channels. This method is based on wave propagation along the winding and measuring the reflection of the wave when a fault occurs. To apply this method, one of the winding terminals is excited by means of a step function and the corresponding transient response at both terminals is measured. The fault detection is done by comparing the faulty response with the healthy response at both terminals. That means that the method requires a previous record of the step response of the healthy transformer at both terminals. It also requires measuring the propagation speed v from the healthy transformer, which can be obtained directly from the previous record of step response at the excitation terminal, according to

$$v = \frac{2LN_l}{t_r} \tag{4.1}$$

where L is the average length of one turn, N_l is the number of turns in the first layer (the one where the excitation is applied), and t_r is the time at which the first reflection is observed in the recorded transient. This reflection is due to the fact that a discontinuity in the winding parameters will appear between the first and second layers. Figure 4.1 shows the recorded response for different permittivities and propagation speeds measured from equation (4.1).

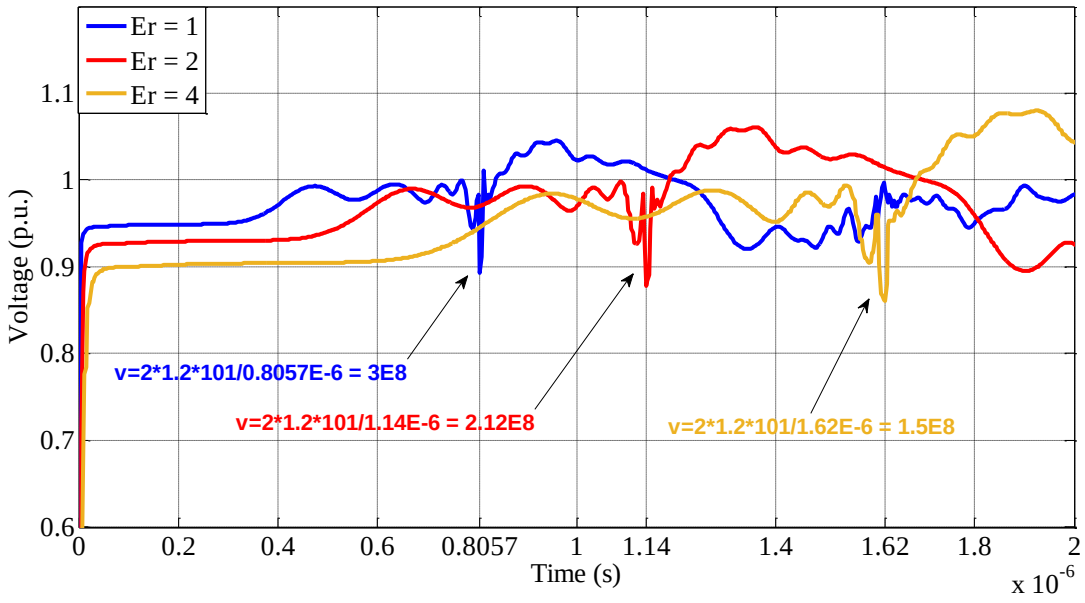

Figure 4.1 Propagation Speed Measurement for different permittivities

In order to obtain general guidelines for the application of the proposed method, several types of faults in a layer-type transformer with different geometrical configurations were simulated using the distributed parameter model described in Chapter 2. This resulted in the flowchart shown in Figure 4.2, which is divided in two parts:

The right-hand part is related to determining the fault location. This requires measuring at the excitation node and locating the first difference (in term of high-frequency oscillations) between the measurement on the faulty transformer and the previously recorded measurement from the healthy transformer. It should be noticed that the response from the healthy transformer already contains oscillations due to the discontinuity between layers. These oscillations should be neglected when performing the comparison. The

equation shown in the right-hand side of the flowchart is used to determine the location of the fault. In this equation, t_f is the time at which the first difference between the faulty and healthy transformer response appears, and x is the location of the fault (the turn number).

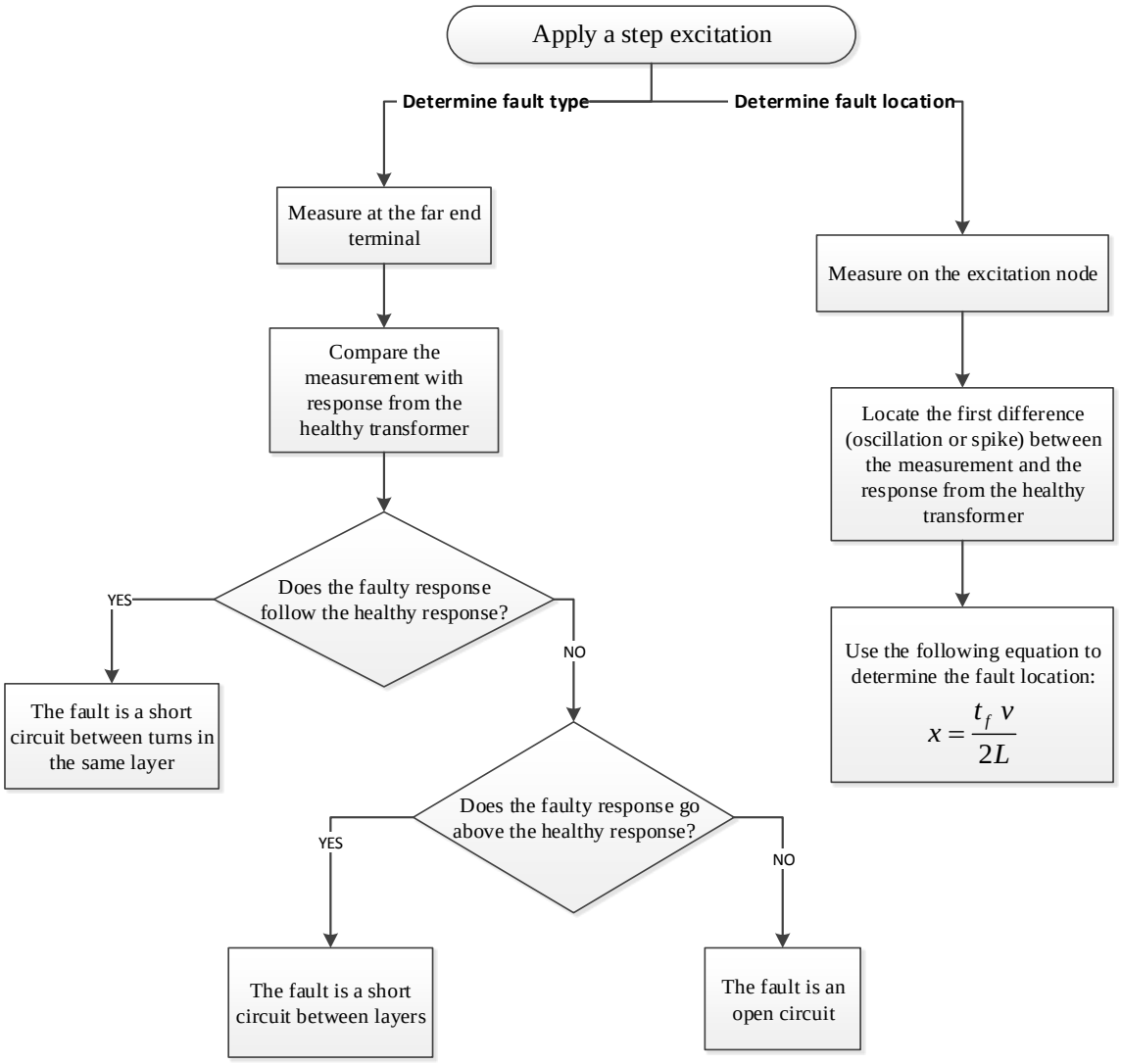

Figure 4.2 Flowchart for the general application of the fault location method

The left-hand part is related to determining the fault type. In order to do that the far end measurement is required. The fault type is determined by comparing the far end measurement from the faulty transformer with the previously recorded measurement from the healthy transformer.

4.3 Test Case Result

The geometrical configuration of the transformer winding shown in Figure 3.5 was used for testing the proposed method. According to Figure 3.5, the winding consists of 303 turns in 3 layers (101 turns per layer). The average length of each turn is 1.2 m.

The following type of faults were applied at different turns of the 3 layers of the transformer winding:

- Short circuit between neighboring turns
- Short circuit between neighboring layers
- Open circuit

The results from these simulations show the type of measurement expected at both winding terminals for different fault conditions. These results are easy to interpret and in complete agreement with the general guidelines provided by the flowchart shown in Figure 4.2.

4.3.1 Short Circuit Fault between Neighboring Turns

Figures 4.3 and 4.4 correspond to the measurement at the excitation node and at the far-end terminal, respectively, when a short circuit fault is applied at layer 1 between turns

50 and 51. It can be seen from Figure 4.3 that the fault produces a noticeable oscillation compared to the healthy response at 0.4 μs. Using the equation from the right-hand side of the flowchart, the location of the fault is determined at turn 50. The propagation speed was measured previously using equation (4.1), and is equal to 3×10^8 m/s.

Figure 4.4 provides information regarding the type of fault by means of a measurement at the far end terminal of the winding. In agreement with the flow chart, when a short circuit fault is applied between neighboring turns from the same layer, the response follows that from the healthy transformer.

Figures 4.5 and 4.6 correspond to the application of a short circuit fault between neighboring turns from the second layer. Figure 4.5 shows that, similarly to the previous case, the short circuit fault produces an oscillation at the excitation node, in this case at 1.04 μs. According to the flowchart, the fault is determined at turn 130, which is consistent with the actual fault location.

Figure 4.6 shows that the response from the far end terminal follows that from the healthy transformer. According to the left hand side of the flowchart, this corresponds to a short circuit fault between neighboring turns in the same layer.

Figures 4.7 and 4.8 show the results from both terminals of the winding when a short circuit fault between turns 235 and 236 (third layer) is applied. Similarly to the previous cases, the proposed method is able to detect the location and type of fault efficiently and accurately.

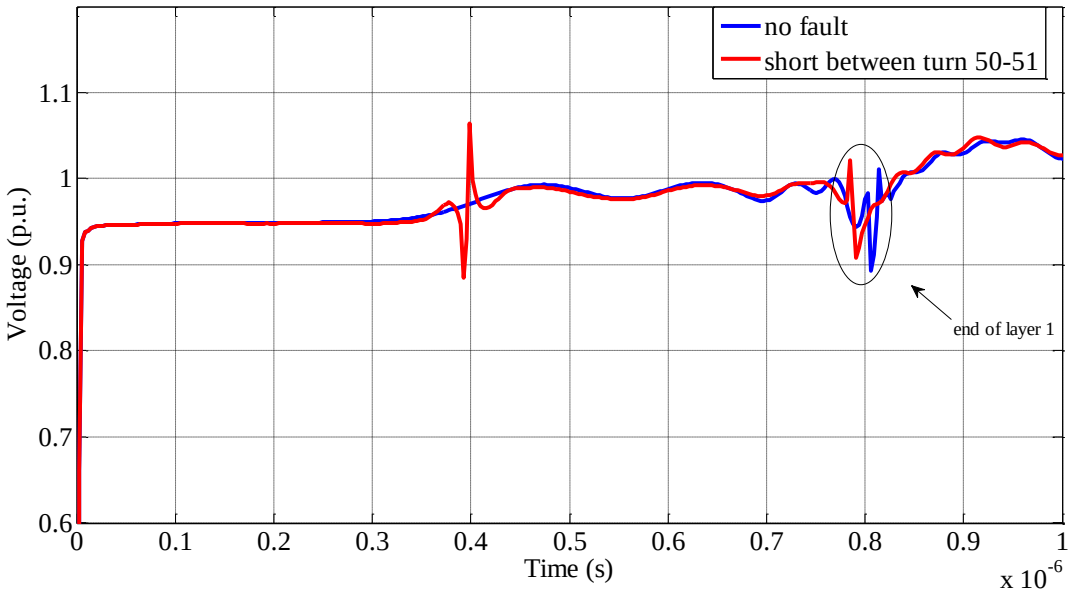

Figure 4.3 Transient voltage response at the excitation node. Short circuit fault at layer 1

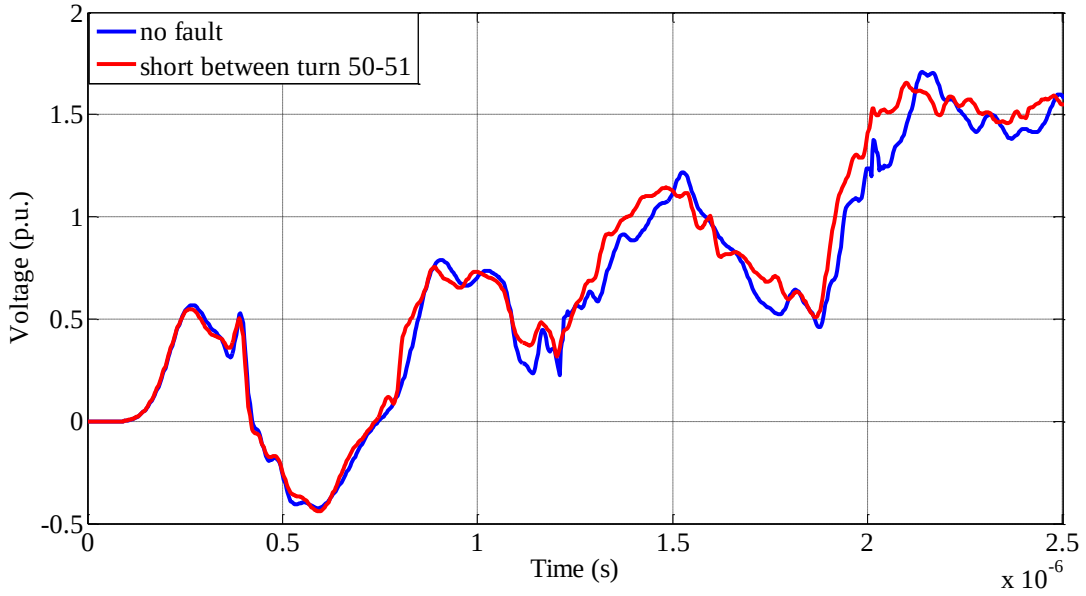

Figure 4.4 Transient voltage response at the far-end node. Short circuit fault at layer 1

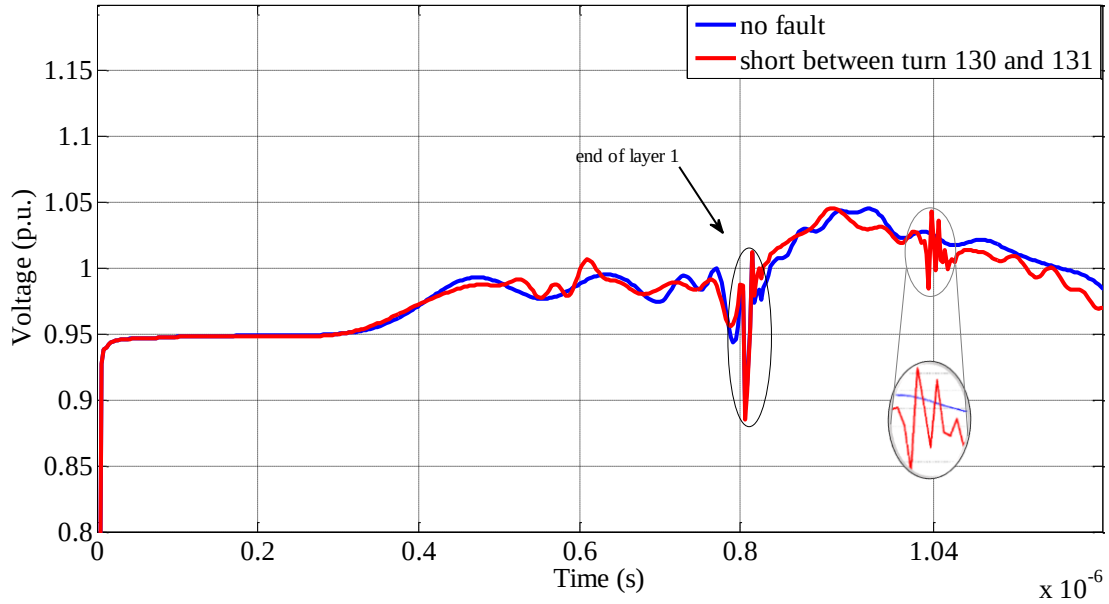

Figure 4.5 Transient voltage response at the excitation node. Short circuit fault at layer 2

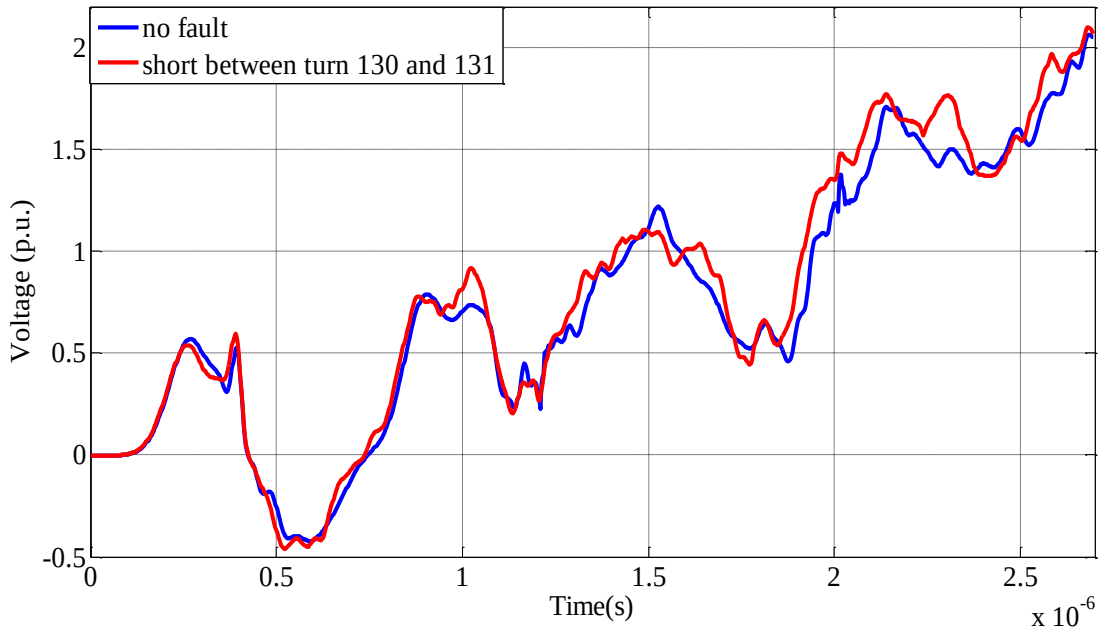

Figure 4.6 Transient voltage response at the far-end node. Short circuit fault at layer 2

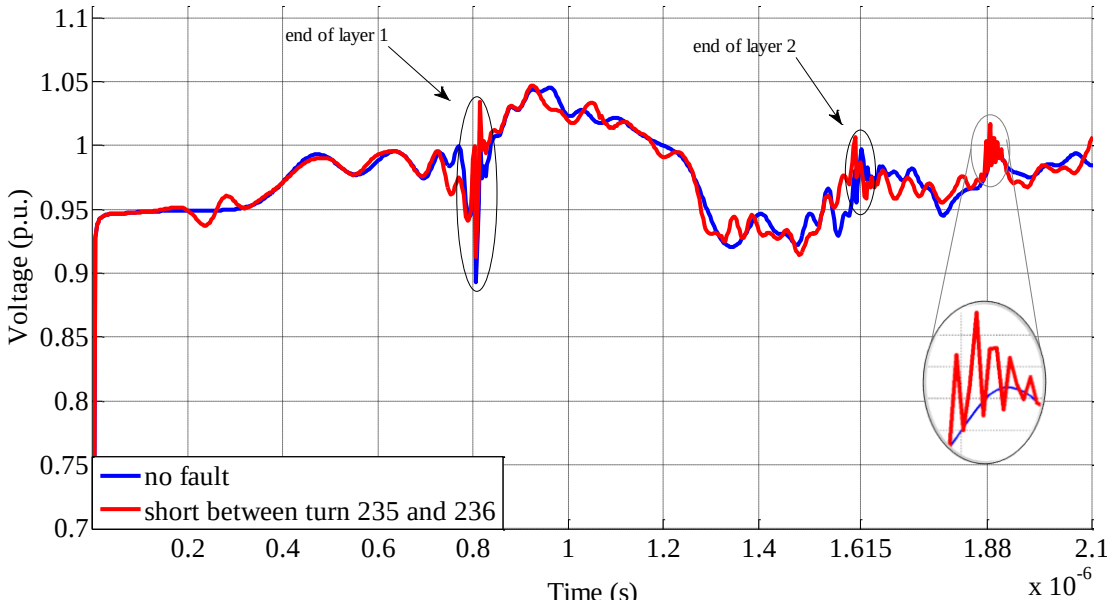

Figure 4.7 Transient voltage response at the excitation node. Short circuit fault at layer 3

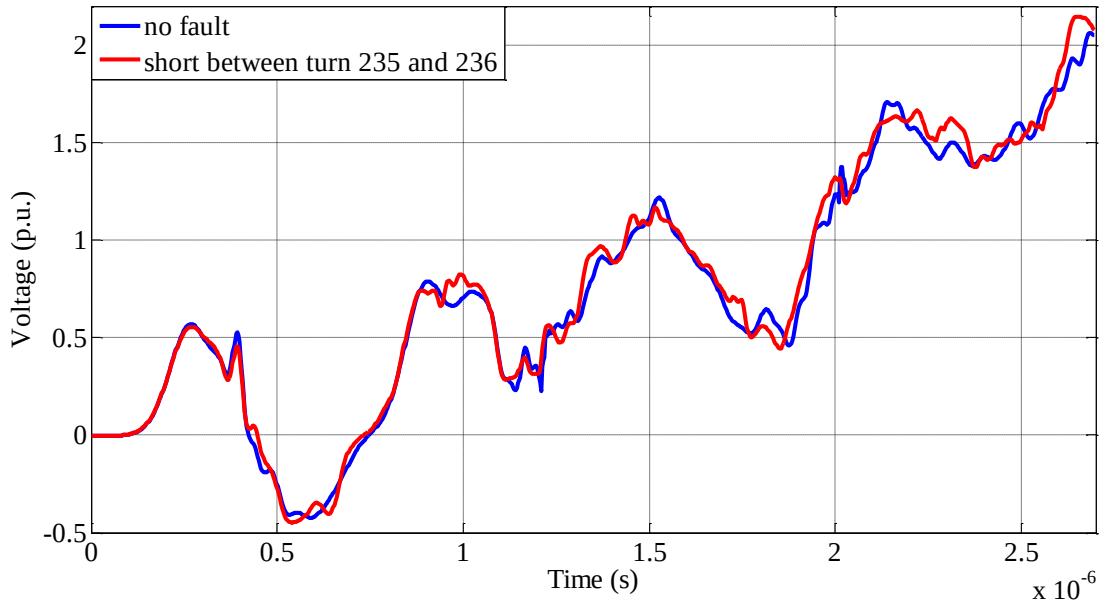

Figure 4.8 Transient voltage response at the far-end node. Short circuit fault at layer 3

4.3.2 Open Circuit Fault

Figures 4.9 and 4.10 show the results obtained at the excitation node and at the far-end terminal of the winding, respectively, when an open circuit fault is applied at layer 1 between turns 50 and 51. Figure 4.9 shows a noticeable oscillation at 0.4 μs, which did not exist in the response from the healthy transformer at the excitation node. Using the flowchart, a value of $x = 50$ is obtained, which is exactly where the fault was applied.

Figure 4.10 provides information regarding the type of the fault by means of a measurement at the far end terminal of the winding. In agreement with the flowchart, when an open circuit fault is applied, the response goes below that from the healthy transformer.

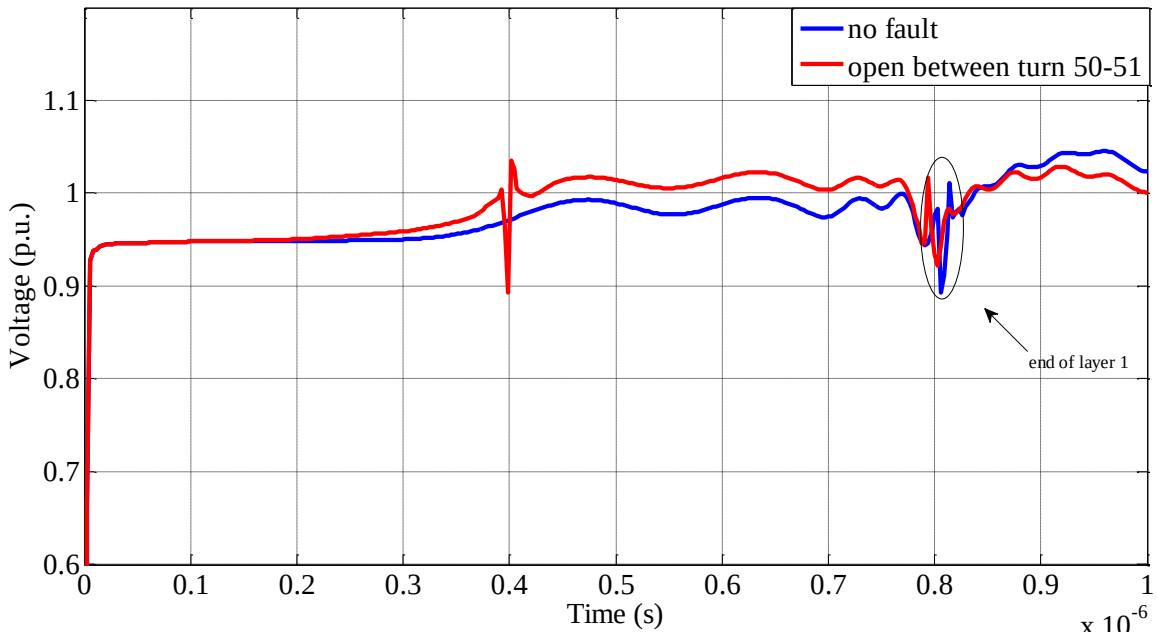

Figure 4.9 Transient voltage response at the excitation node. Open circuit fault at layer 1

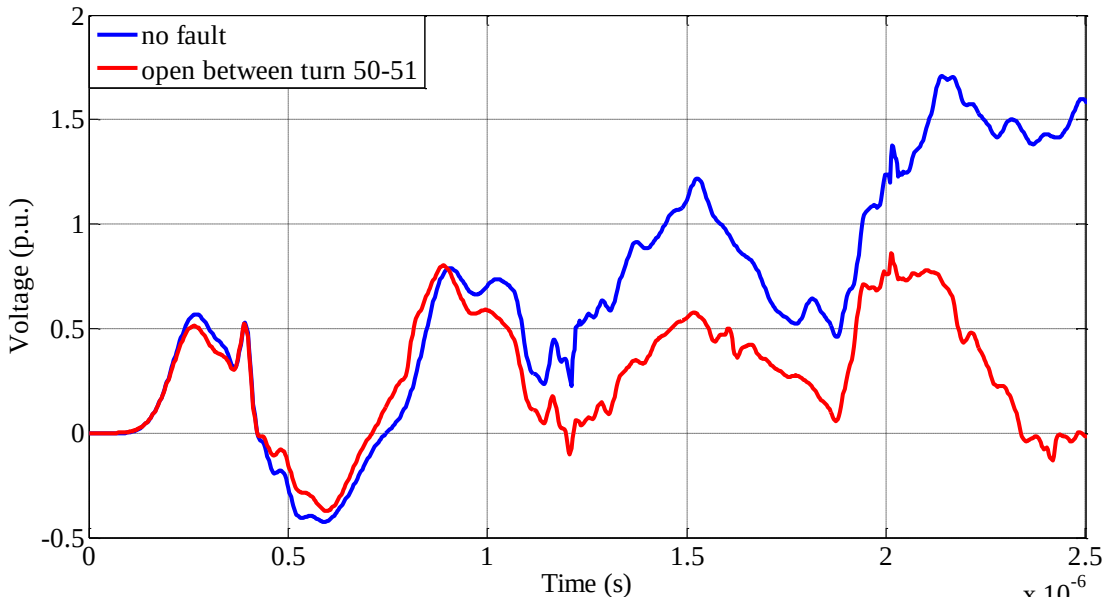

Figure 4.10 Transient voltage response at the far-end node. Open circuit fault at layer 1

As it can be seen in Figures 4.11 and 4.12, similar results are obtained when an open circuit fault is applied between turns 130 and 131, corresponding to the second layer. According to Figure 4.11, an oscillation appears at 1.04 μs when the fault is applied. From the flowchart, the fault location is determined at turn 130. Figure 4.12 shows that the response from the far end terminal goes below that from the healthy transformer, corresponding to an open circuit condition.

Figures 4.13 and 4.14 show the results when an open circuit fault is applied between turns 255 and 256 (third layer). An oscillation at 2.04 μs is shown in Figure 4.13, while Figure 4.14 shows that the far end response goes below the heathy response.

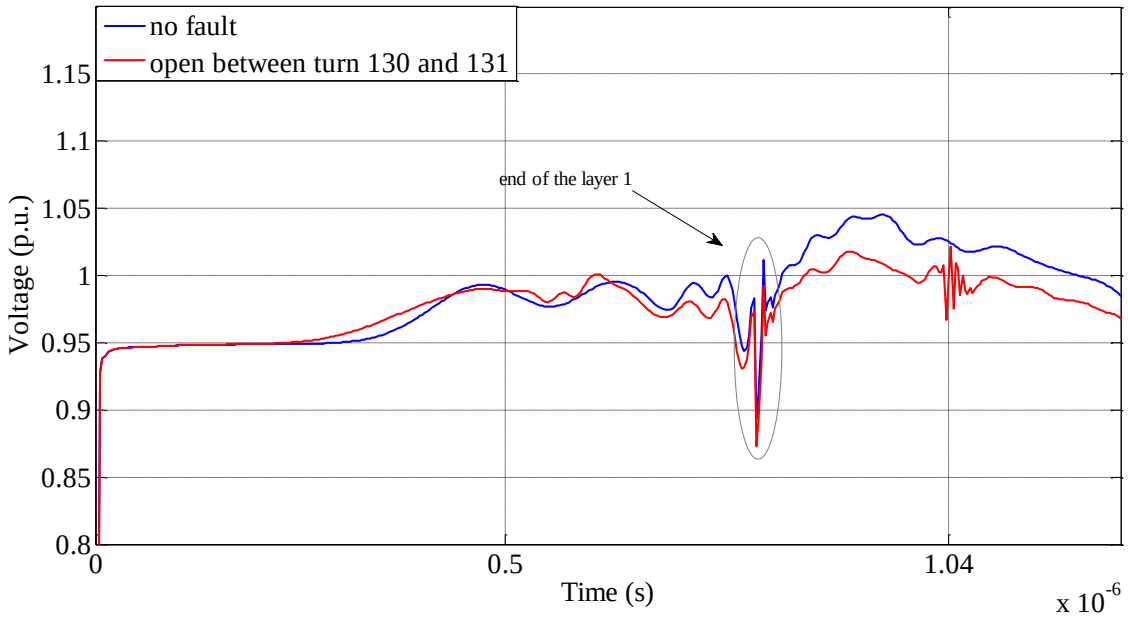

Figure 4.11 Transient voltage response at the excitation node. Open circuit fault at layer 2

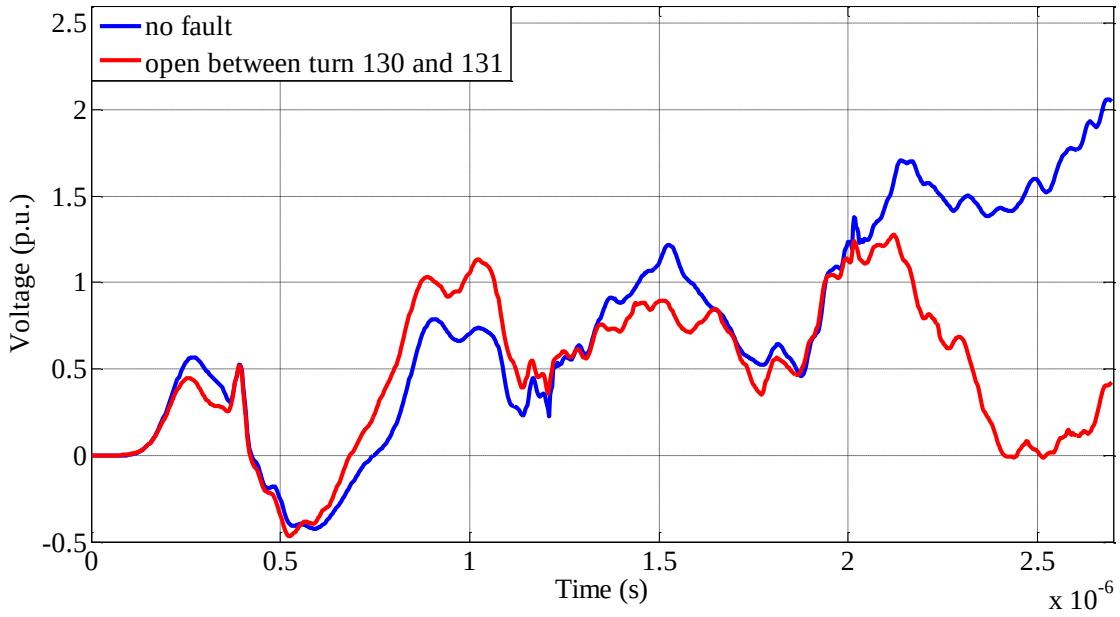

Figure 4.12 Transient voltage response at the far-end node. Open circuit fault at layer 2

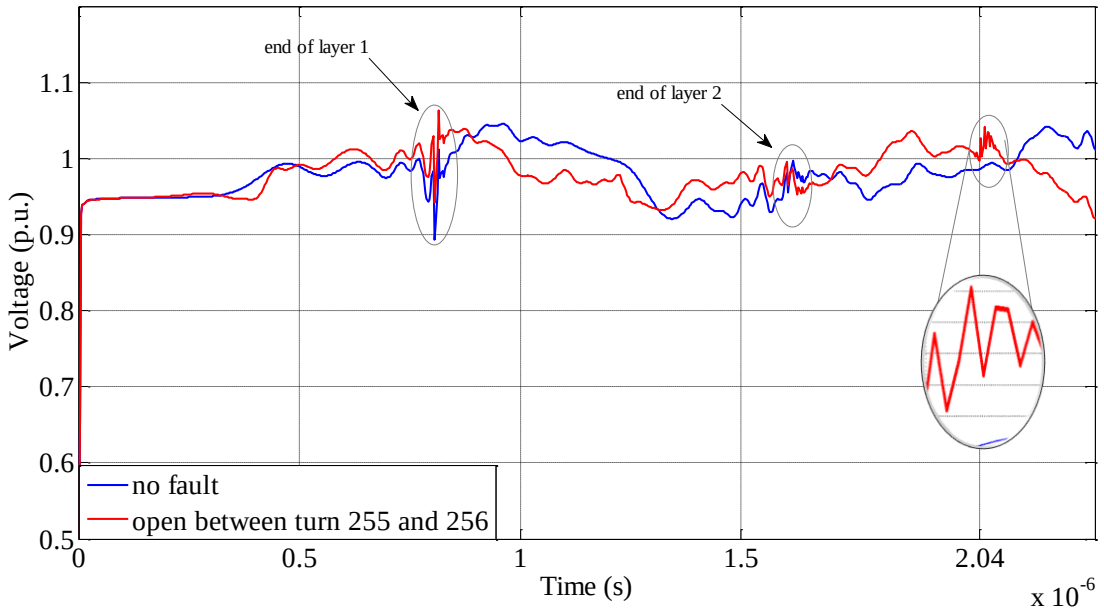

Figure 4.13 Transient voltage response at the excitation node. Open circuit fault at layer 3

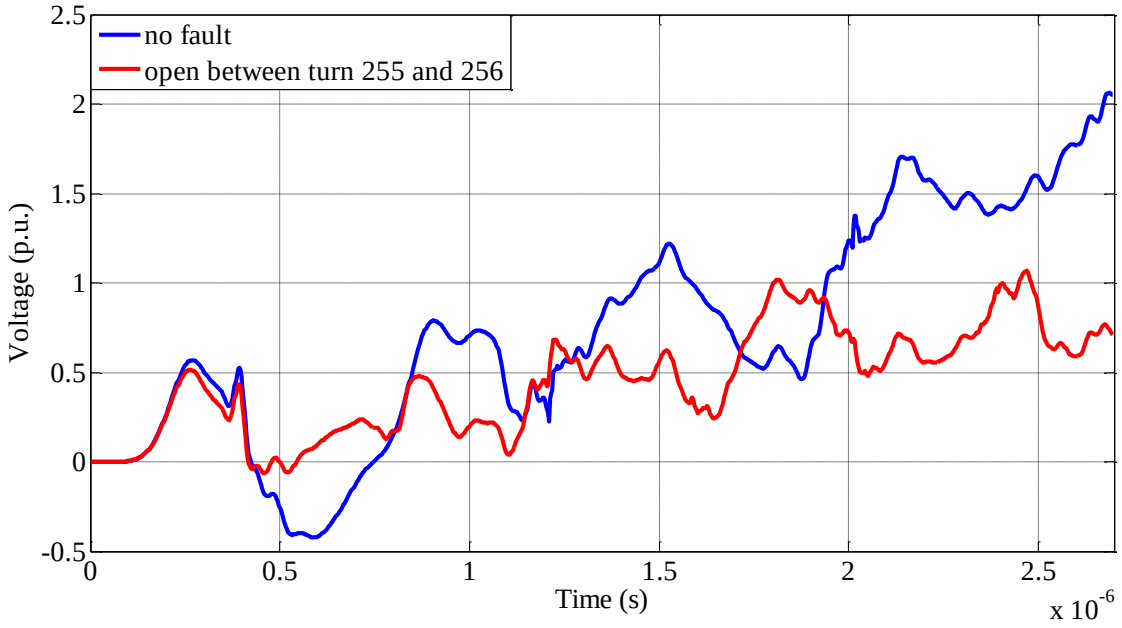

Figure 4.14 Transient voltage response at the far-end node. Open circuit fault at layer 3

4.3.3 Short Circuit Fault between Neighboring Layers

Figures 4.15 and 4.16 show the transient response of the winding at the excitation node and at the far-end terminal, respectively, when a short circuit fault is applied between layers 1 and 2. Figure 4.9 shows that the fault application results in an oscillation at 0.4365 μs in the excitation node. From the flowchart, $x = 55$, which corresponds to the actual fault location.

Figure 4.16 shows that the faulty response goes above the healthy response, which means that the fault occurs between neighboring layers.

Figures 4.17 and 4.18 correspond to the measurements at the excitation node and at the far-end terminal, respectively, when a short circuit fault is applied between layers 2 and 3. Figure 4.17 shows the appearance of an oscillation at 1.025 μs in the excitation node response when the fault is applied. In this case, a value of $x = 128$ is obtained. This is again the exact location of the fault.

From Figure 4.18, the measurement at the far end node of the faulty transformer goes above that from the healthy transformer. Similarly to the previous case, this corresponds to a short circuit fault between neighboring layers.

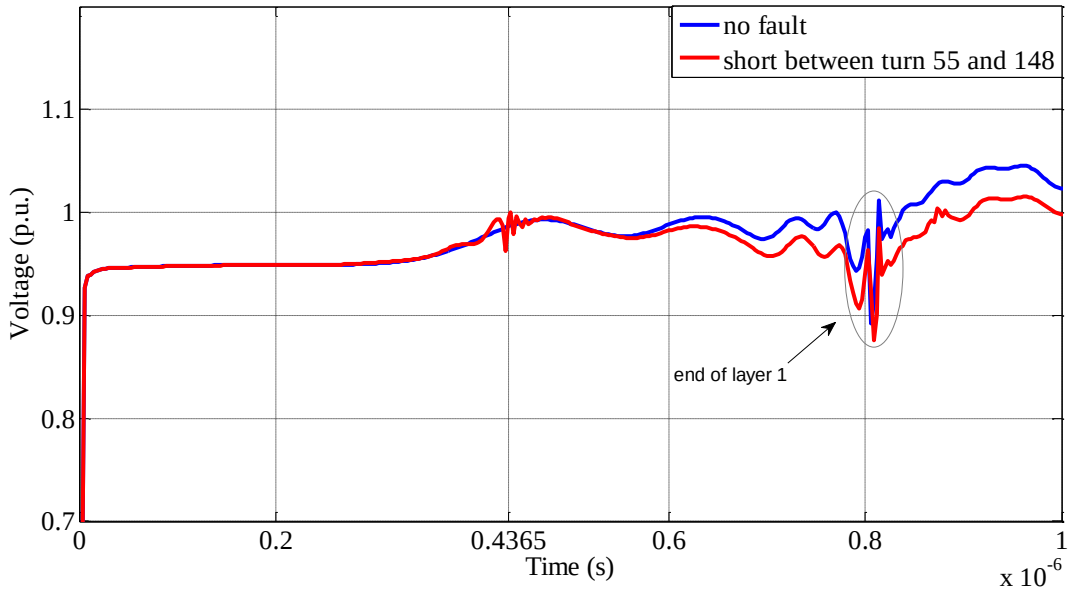

Figure 4.15 Transient voltage response at the excitation node. Short circuit fault between layers 1 and 2

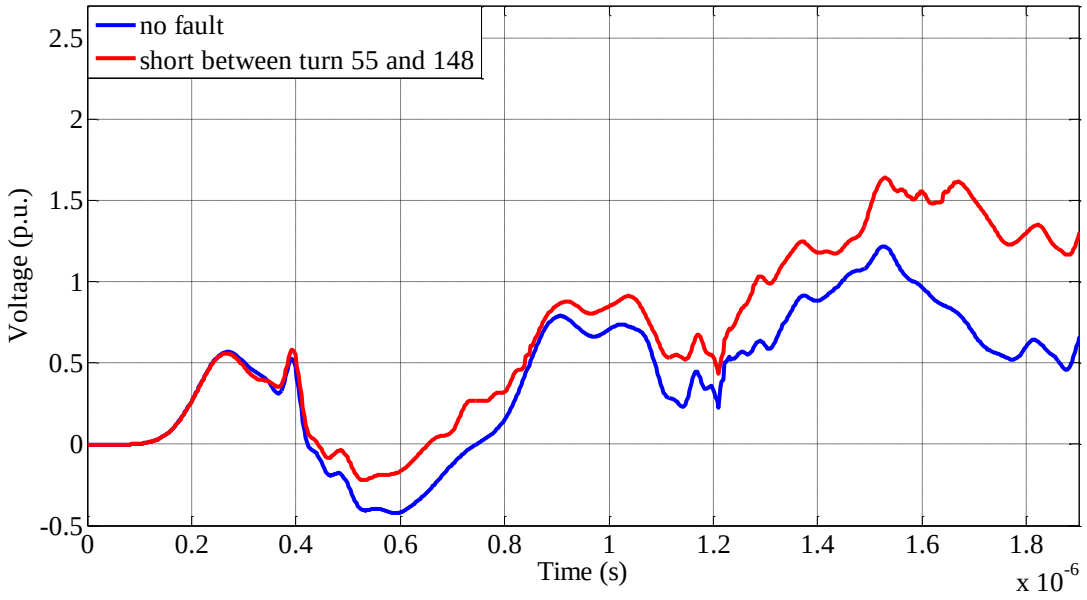

Figure 4.16 Transient voltage response at the far-end node. Short circuit fault between layers 1 and 2

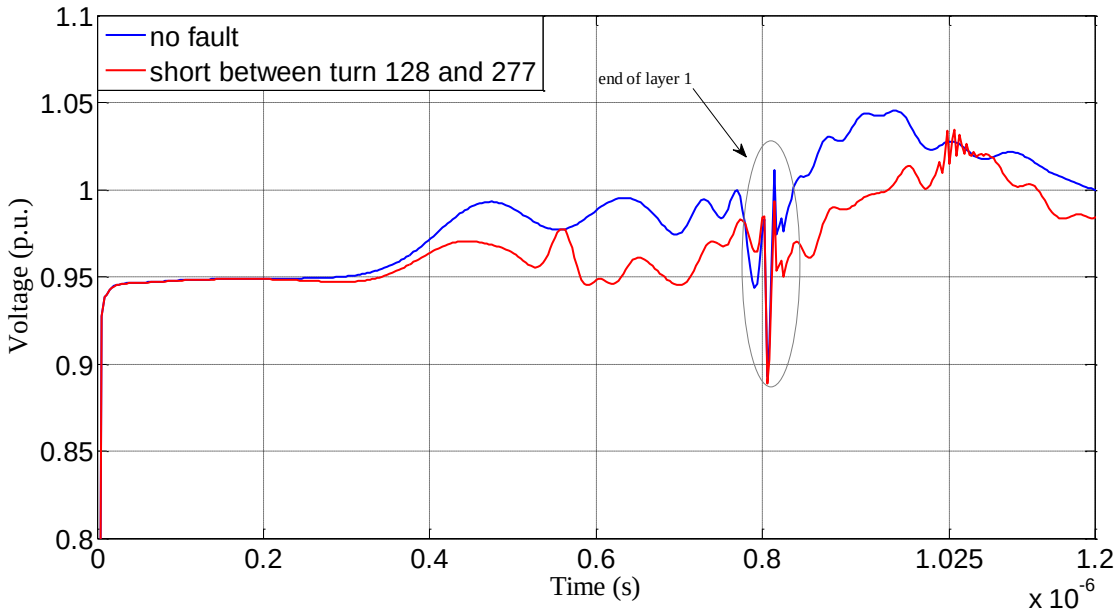

Figure 4.17 Transient voltage response at the excitation node. Short circuit faults between layers 2 and 3

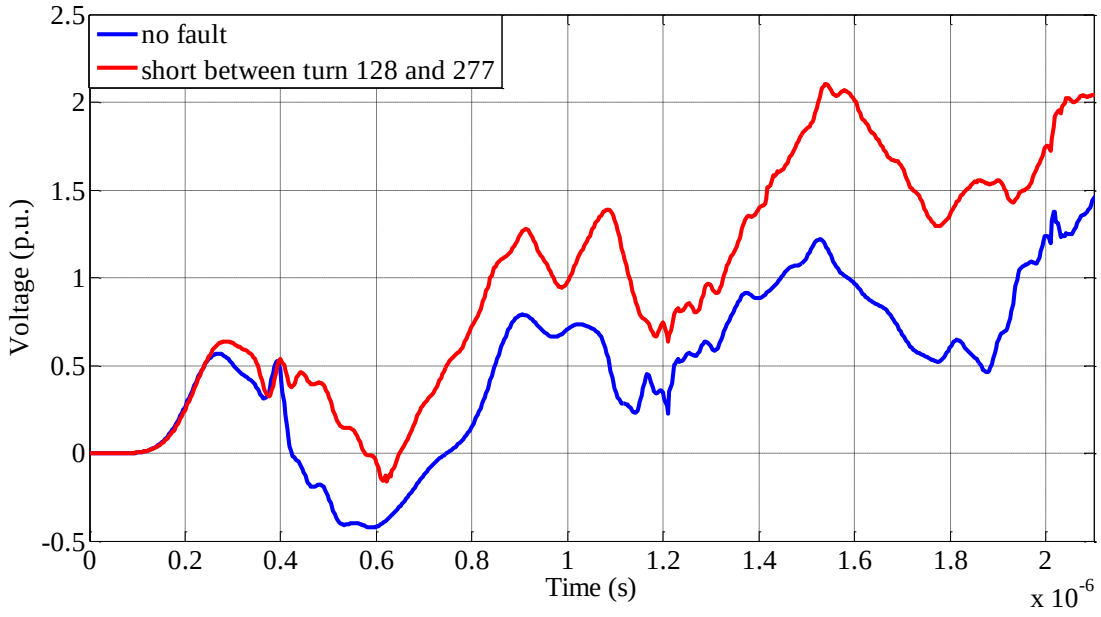

Figure 4.18 Transient voltage response at the far-end node. Short circuit faults between layers 2 and 3

4.3.4 Comparison between Different Fault Types

Figures 4.19 and 4.20 correspond to the measurements at the excitation node and at the far end terminal, respectively, when different types of faults are applied at turn 50. From Fig. 4.19, it can be seen that all types of faults produce a noticeable oscillation at 0.4 μs, which did not exist in the response from the healthy transformer at the excitation node. With the simple formula provided on the right-hand side of the flow-chart, a value of $x = 50$ is obtained, which matches the faulted turn for all fault types. A further oscillation can be noticed at around 0.8 μs. However, this oscillation already existed in the healthy transformer and is due to the end of the first layer.

Figure 4.20 provides information regarding the type of fault, by means of measurements at the far end terminal of the winding. In agreement with the flow chart, when a short circuit fault is applied between neighboring turns from the same layer, the response follows that from the healthy transformer. On the other hand, a short circuit between layers and an open circuit produce waveforms with magnitudes above and below the response from the healthy transformer, respectively.

A similar set of simulations was performed considering different types of faults in the second layer. The results are shown in Figures 4.21 and 4.22. Analyzing the measurements at both ends of the winding, the results are very similar to the previous case (faults on the first layer). In this case, a value of $x = 152$ is obtained.

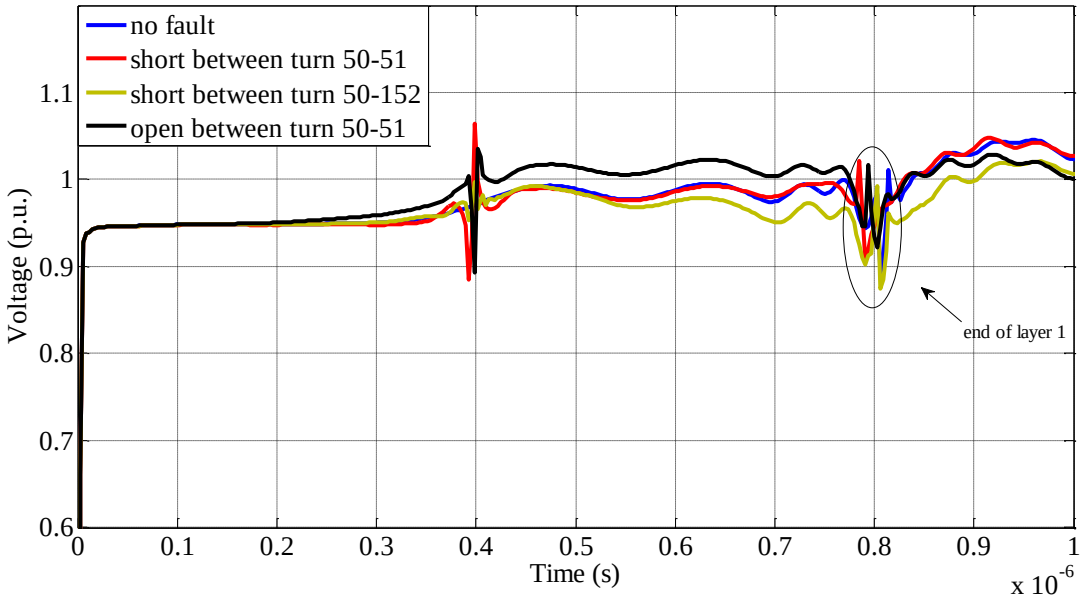

Figure 4.19 Transient voltage response at the excitation node. Faults at layer 1

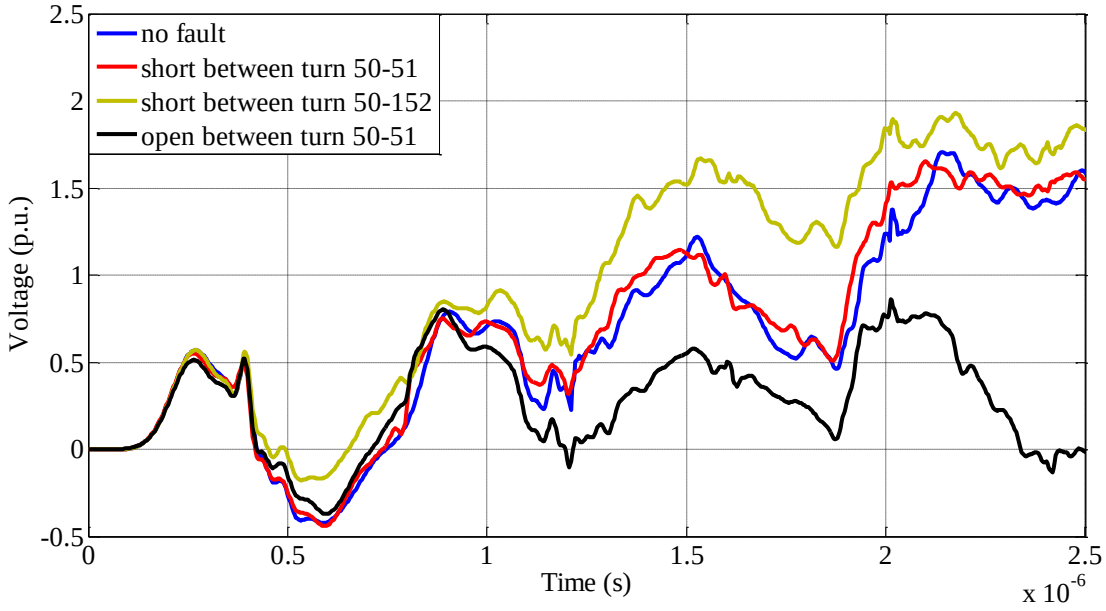

Figure 4.20 Transient voltage response at the far-end node. Faults at layer 1

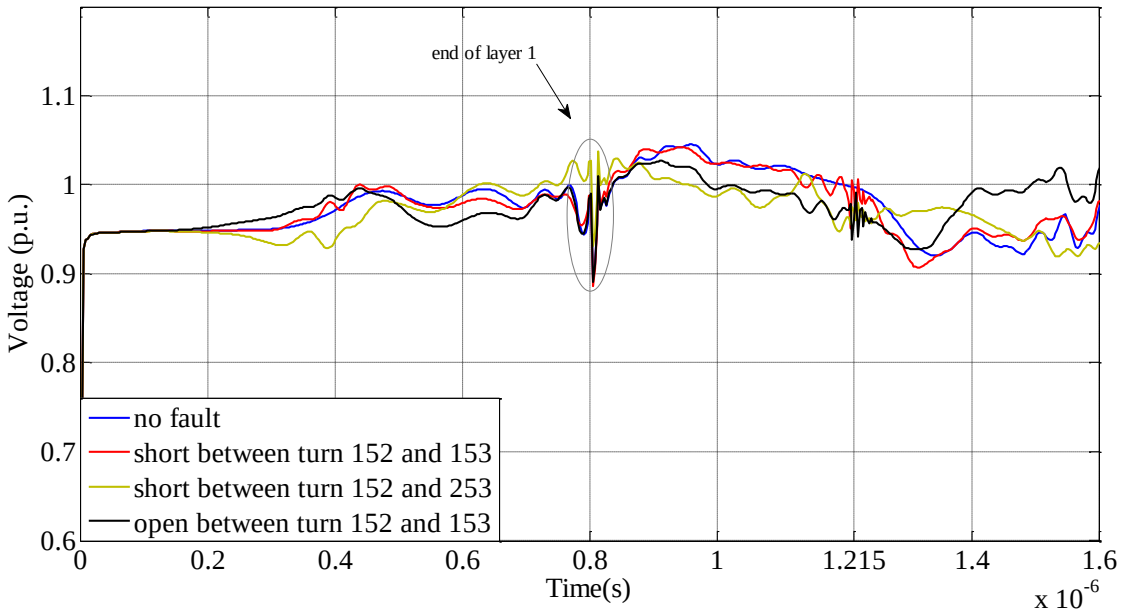

Figure 4.21 Transient voltage response at the excitation node. Faults at layer 2

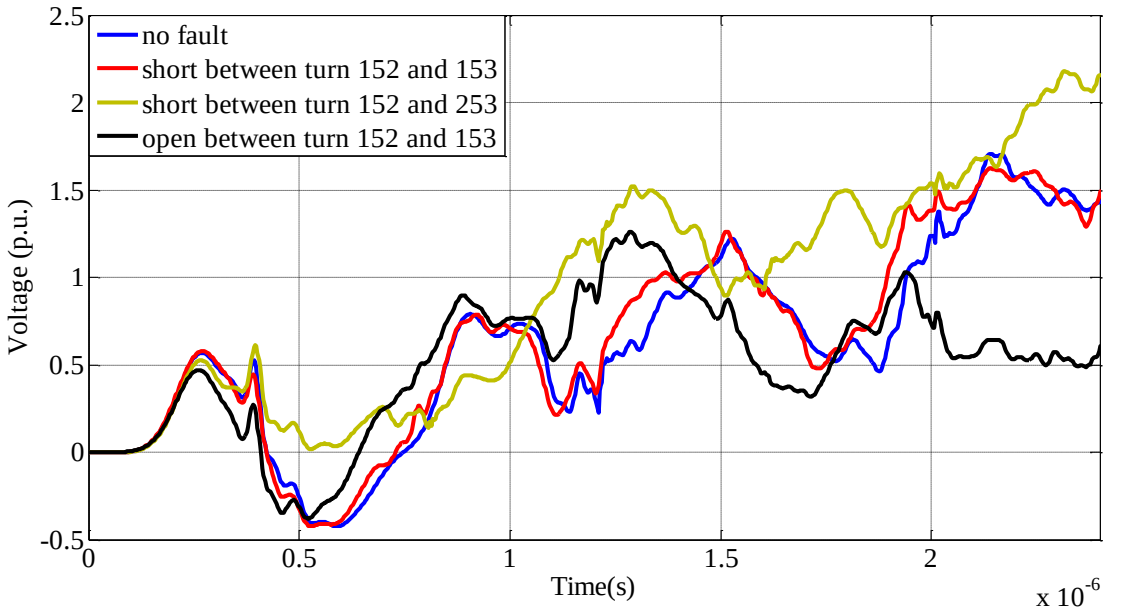

Figure 4.22 Transient voltage response at the far-end node. Faults at layer 2

CHAPTER 5

CONCLUSIONS AND FUTURE WORK

An accurate and cost-effective fault detection method for power transformer is very important to avoid further delays in the network operation. This thesis presents and evaluates a time domain method to locate and classify internal faults in transformer windings, which is based on wave propagation and reflection along windings subjected to different type of faults. The general procedure of the proposed method is defined by means of a flowchart related to a step excitation at one of the winding terminals and measurements at both terminals. Therefore, the method is very simple and requires accessible and low-cost lab equipment.

The effectiveness of the method is tested by means of simulations on a transformer winding with 303 turns in 3 layers (101 turns per layer). The method is able to identify the type and location of different types of faults and at different turns along the winding with high accuracy. The analytical and simulation results in this thesis yield the following conclusions:

1. It is possible to detect and locate faults in a transformer winding with low-cost equipment (low voltage DC source or waveform generator and oscilloscope with two output channels). The proposed method is simple and yet very accurate.

2. A distributed-parameter model is applied to predict the transient response of transformer winding under different internal fault conditions. This type of model allows predicting the wave propagations along a winding with better accuracy than a lumped-parameter model.
3. A frequency domain model was used, since it allows introducing the frequency dependence of the winding parameters in a straightforward manner. This feature is essential for an accurate prediction of the damping effect and distortion of the transient response of the winding.
4. Parameter determination is one of the most important parts of the model in order to have an accurate prediction of the transformer winding response. One of the most accurate ways to determine the winding parameters is by using an electromagnetic simulation software based on the finite element method. Commercial software COMSOL Multiphysics 5.1 was used for this purpose.
5. The proposed method requires a previous record of step response from the healthy transformer. This record can be provided by the manufacturer, or it can be recorded by the user before putting the transformer in service. For 3-phase transformers, this response can be registered from one of the other phases if the fault condition is only observed at one phase.
6. Propagation speed is also required to perform this method. This can be provided by the manufacturer or measured directly from the previous record on the healthy transformer.

Concerning recommendations for future work, the following list is provided:

1. Validating this method with tests on a real layer-type transformer.
2. Extending the proposed method to disc-type transformers.
3. Developing new alternatives to process the measurement results in order to make the fault location even more straightforward. Different signal processing techniques could be applied for this purpose.
4. Short and open circuit faults are the most common faults, but there are other types of relevant fault conditions. It is recommended to improve the method to be able to detect and classify other type of conditions, such as mechanical deformations or partial faults.

BIBLIOGRAPHY

[1] J. M. Vilanueva-Ramirez, "Implementation of transformers models for high-frequency electromagnetic analysis," National Polytechnic Institute, Mexico city, 2013.

[2] M. Mahvi and V. Behjat, "Localising low-level short-circuit faults on the windings of power transformers based on low-frequency response measurement of the transformer windings," *Electric Power Applications, IET,* vol. 9, no. 8, pp. 553-539, 2015.

[3] I. J. T. F. o. Q. E. Review, "IEEE Report to DOE QER Priority Issues," Prepared for W. F. Hederman, Senior Adviser of the Secretary, US Dept. of Energy, Washington DC, September 5, 2014.

[4] I. A. Metwally, "Failures, Monitoring and New Trends of Power Transformers,," *IEEE Potentials,* vol. 30, no. 3, pp. 36-43, May 2011.

[5] M. Taikina-aho, "Survey of transformer failure causes and consequences," Bachelor of Science and Technology Thesis, University of Vaasa, Finland, 2010.

[6] L. Rabins, "A New Approach to the Analysis of Impulse Voltages and Gradients in Transformer Windings," *Power Apparatus and Systems, Part III. Transactions of the American Institute of Electrical Engineers,* vol. 78, no. 4, pp. 1784 - 1791, 1959.

[7] Y. Shibuya, S. Fujita and N. Hosokawa, "Analysis of very fast transient overvoltage in transformer winding," *Generation, Transmission and Distribution, IEE Proceedings,* vol. 144, no. 5, pp. 461 - 468, 1997.

[8] Y. Shibuya, S. Fujita and E. Tamaki, "Analysis of very fast transients in transformers," *Generation, Transmission and Distribution, IEE Proceedings,* vol. 148, no. 5, pp. 377 - 383, 2001.

[9] Y. Shibuya and S. Fujita, "High frequency model and transient response of transformer windings," in *Transmission and Distribution Conference and Exhibition 2002: Asia Pacific. IEEE/PES,* 2002.

[10] A. S. Alfuhaid, "Frequency characteristics of single-phase two-winding transformers using distributed-parameter modeling," *Power Delivery, IEEE Transactions,* vol. 16, no. 4, pp. 637 - 642, 2001.

[11] G. Liang, H. Sun, X. Zhang and X. Cui, "Modeling of Transformer Windings Under Very Fast Transient Overvoltages," *Electromagnetic Compatibility, IEEE Transactions,* vol. 48, no. 4, pp. 621 - 627, 2006.

[12] M. Popov, L. van der Sluis, R. P. Smeets and J. Lopez-Roldan, "Modelling, simulation and measurement of fast transients in transformer windings with consideration of frequency-dependent losses," *Electric Power Applications, IET,* vol. 1, no. 1, pp. 29 - 35, 2007.

[13] X. Zhu, H. Dong, G. Liang and C. Ji, "A new hybrid model of transformer windings under very fast transient overvoltages," in *Electrical Machines and Systems, 2008. ICEMS 2008. International Conference,* Wuhan, 2008.

[14] J. M. Villanueva-Ramírez, . P. Gómez, F. . P. Espino-Cortés and . G. Nájera, "Implementation of time domain transformer winding models for fast transient analysis using Simulink," *International Journal of Electrical Power & Energy Systems,* vol. 61, p. 118–126, October 2014.

[15] F. de Leon and A. Semlyen, "Efficient calculation of elementary parameters of transformers," *Power Delivery, IEEE Transactions,* vol. 7, no. 1, pp. 376 - 383, 1992.

[16] X. Yan, W. Zengping and L. Qing, "A Novel Inductance Calculation Method in Power Transformer Model Based on Magnetic Circuit," in *TENCON 2005 2005 IEEE Region 10,* Melbourne, Qld., 2005.

[17] Y. Li, J. Du, X. Li and D. Li, "Calculation of capacitance and inductance parameters based on FEM in high-voltage transformer winding," in *Electrical Machines and Systems (ICEMS), 2011 International Conference,* Beijing, 2011.

[18] P. Gomez and F. de León, "Accurate and Efficient Computation of the Inductance Matrix of Transformer Windings for the Simulation of Very Fast Transients," *Power Delivery, IEEE Transactions,* vol. 26, no. 3, pp. 1423-1431, 2011.

[19] P. Gomez, F. de Leon and F. P. Espino-Cortes, "Improvement of a Method to Compute the Inductance Matrix of Multilayer Transformer Windings for Very Fast

Transients," *Power Delivery, IEEE Transactions,* vol. 28, no. 2, pp. 1245 - 1246, 2013.

[20] M. Eslamian and B. Vahidi, "New Methods for Computation of the Inductance Matrix of Transformer Windings for Very Fast Transients Studies," *Power Delivery, IEEE Transactions*, vol. 27, no. 4, pp. 2326 - 2333, 2012.

[21] A. De and N. chatterjee, "Impulse fault diagnosis in power transformers using self-organising map and learning vector quantisation," *Generation, Transmission and Distribution, IEE Proceedings,* vol. 148, no. 5, pp. 397-405, 2001.

[22] S. Nandi, "A Novel Frequency Domain Based Technique to Detect Transformer Inter-turn Faults," in *Electric Machines & Drives Conference, 2007. IEMDC '07. IEEE International* , Antalya, 2007.

[23] N. Yadaiah and N. Ravi, "Fault Detection Techniques for Power Transformers," in *Industrial & Commercial Power Systems Technical Conference, 2007. ICPS 2007. IEEE/IAS*, Edmonton, Alta., 2007.

[24] O. Aljohani and A. Abu-Siada, "Minimum detection of power transformer short circuit fault using frequency response analysis," in *Power Engineering Conference (AUPEC), 2015 Australasian Universities*, Wollongong, Australia, 2015.

[25] Z. Zhang, . W.-H. Huang, D.-M. Xiao and Y.-L. Liu, "Fault detection of power transformers using genetic programming method," *Machine Learning and Cybernetics, 2004. Proceedings of 2004 International Conference*, vol. 5, pp. 3018-3022, 2004.

[26] A. Greenwood, Electrical Transients in Power Systems, John Wiley & sons, Inc, 1991.

[27] F. de leon, P. Gomez, j. A. Martinez-Velasco and M. Rioual, "chapter 4, Transformers," in *Power System Transients: parameter Determination(Edited by J. A. Mrtinez-Velasco)*, Boca Raton FL, CRC Press, 2009, pp. 177-250.

[28] P. Gomez, Writer, *Modeling of Power Equipment for Electromagnetic Transient Analysis [PowerPoint slides]*. [Performance]. Western Michigan University, 2015.

[29] P. Ying and R. Jiangjun, "Investigation of Very Fast Transient Overvoltage Distribution in Taper Winding of Tesla Transformer," *Magnetics, IEEE Transactions on,* vol. 42, no. 3, pp. 434 - 441, 2006.

[30] C. Q. Su, Electromagnetic Transient in Transformer and Rotating Machine Windings, Hershey, PA: Information Science Reference, 2013.

[31] M. Popov, L. Van der Sluis, G. C. Paap and H. de Herdt, "Computation of Very Fast Transient Overvoltages in Transformer Windings," *Power Engineering Review, IEEE*, vol. 22, no. 10, pp. 62-62, 2002.

[32] S. V. Kulkarni and S. A. Khaparde, Transformer Engineering Design and Practice, NEW YORK: MARCEL DEKKER, INC, 2005.

[33] J. Du, G. Liang, H. Sun, X. Liu and X. Liu, "Lumped parameter modeling of transformer windings under VFTO," in *Microwave, Antenna, Propagation, and EMC Technologies for Wireless Communications (MAPE), 2011 IEEE 4th International Symposium on*, Beijing, 2011.

[34] M. Popov, L. van der Sluis, R. P. Smeets, J. Lopez-Roldan and V. V. Terzija, "Modelling, simulation and measurement of fast transients in transformer windings with consideration of frequency-dependent losses," *IET Electric Power Appl.*, vol. 1, no. 1, pp. 29-35, Jan. 2007.

[35] W. H. Hayt and J. A. Buck, Engineering Electromagnetics, Mexico: McGaw Hill, 2012.

[36] A. Miki, T. Hosoya and K. Okuyama, "A Calculation Method for Impulse Voltage Distribution and Transferred Voltage in Transformer Windings," *Power Apparatus and Systems, IEEE Transactions on*, Vols. PAS-97, no. 3, pp. 930-939, 1978.

[37] P. Gomez, F. de Leon and I. A. Hernandez, "Impulse-Response Analysis of Toroidal Core Distribution Transformers for Dielectric Design," *Power Delivery, IEEE Transactions on*, vol. 26, no. 2, pp. 1231-1238, 2011.

[38] A. J. Thomas and S. M. Mahajan, "Capacitive weighting technique for estimating the 3D turn-level capacitance in a transformer winding," *ELSEVIER Electric Power Systems Research*, vol. 81, no. 1, pp. 117-122, 2011.

[39] Z. Azzouz, A. Foggia, L. Pierrat and G. Meunier, "3D finite element computation of the high frequency parameters of power transformer windings," *Magnetics, IEEE Transactions*, vol. 29, no. 2, pp. 1407-1410, 2002.

[40] C. R. Paul, "Decoupling the Multiconductor Transmission Line Equations," *Microwave Theory and Techniques, IEEE Transactions,* vol. 44, no. 8, pp. 1429 - 1440, Aug 1996.

[41] G. Liang, H. Sun, X. Zhang and X. Cui, "Modeling of Transformer Windings Under Very Fast Transient Overvoltages," *Electromagnetic Compatibility, IEEE Transactions,* vol. 48, no. 4, pp. 621 - 627, Nov. 2006.

[42] M. M. Kane and S. V. Kulkarni, "MTL-Based Analysis to Distinguish High-Frequency Behavior of Interleaved Windings in Power Transformers," *Power Delivery, IEEE Transactions,* vol. 28, no. 4, pp. 2291 - 2299, 09 July 2013.

[43] S. M. Hosseini, M. Vakilian and G. B. Gharehpetian, "Comparison of Transformer Detailed Models for Fast and Very Fast Transient Studies," *Power Delivery, IEEE Transactions,* vol. 23, no. 2, pp. 733 - 741, April 2008.

[44] P. Gómez, J. C. Escamilla and P. Moreno, "Time domain distributed parameter modeling of transformer windings for fast front transients," in *10th international conference on power systems transients (IPST'13),* Vancouver, Canada., 2013.

[45] M. Popov, L. van der Sluis, R. P. Smeets and J. L. Roldan, "Analysis of Very Fast Transients in Layer-Type Transformer Windings," *Power Delivery, IEEE Transactions,* vol. 22, no. 1, pp. 238-247, 2007.

[46] C. R. Paul, "Decoupling the multiconductor transmission line equations," *Microwave Theory and Techniques, IEEE Transactions,* vol. 44, no. 8, pp. 1429-1440, 1996.

[47] S. M. Islam, "Detection of shorted turns and winding movements in large power transformers using frequency response analysis," *Power Engineering Society Winter Meeting, 2000. IEEE,* vol. 3, pp. 2233 - 2238, 2000.

Appendix A: COMSOL Results

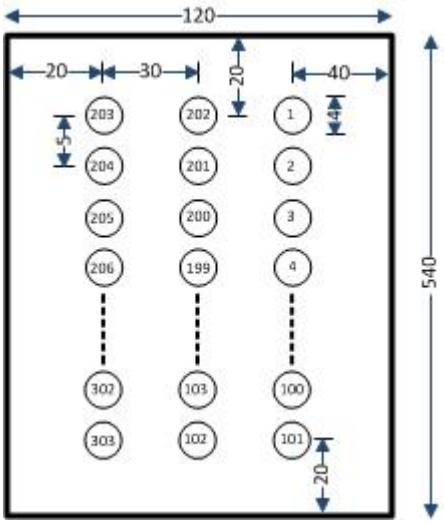

Figure A. 1 Configraution for three layer transformer winding

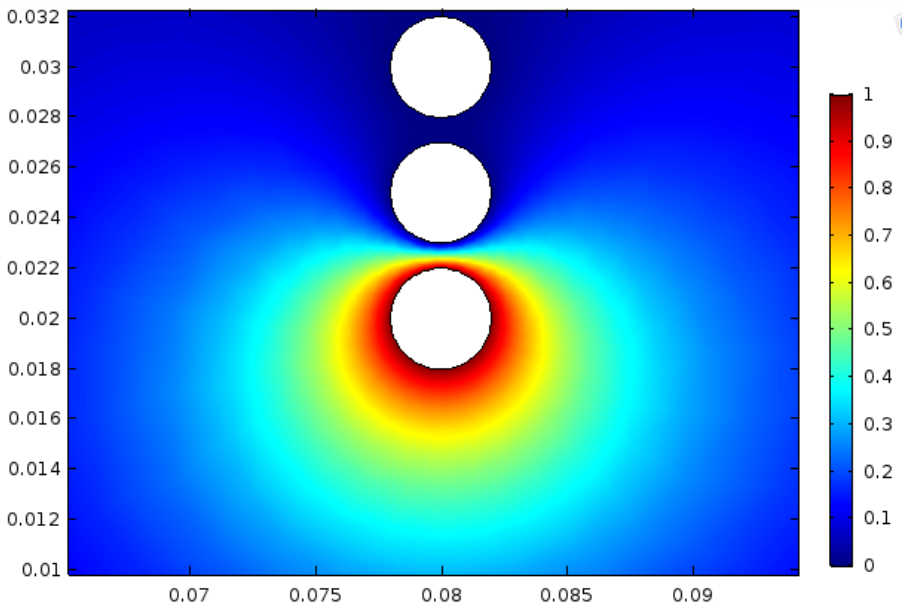

Figure A. 2 COMSOL Multiphysics simulation (electric potential)

Turn	1	2	3	4	5
1	4.73e-11	-3.25e-11	-1.91e-12	-7.54e-13	-3.71e-13
2	-3.25e-11	7.09e-11	-3.14e-11	-1.52e-12	-5.64e-13
3	-1.91e-12	-3.14e-11	7.10e-11	-3.14e-11	-1.51e-12
4	-7.54e-13	-1.52e-12	-3.14e-11	7.10e-11	-3.14e-11
5	-3.71e-13	-5.64e-13	-1.51e-12	-3.14e-11	7.10e-11
6	-2.02e-13	-2.70e-13	-5.58e-13	-1.50e-12	-3.14e-11
7	-1.15e-13	-1.44e-13	-2.66e-13	-5.57e-13	-1.50e-12
8	-6.87e-14	-8.22e-14	-1.42e-13	-2.66e-13	-5.57e-13
9	-4.17e-14	-4.85e-14	-8.11e-14	-1.42e-13	-2.66e-13
10	-2.57e-14	-2.93e-14	-4.78e-14	-8.09e-14	-1.42e-13

Table A. 1 Capacitive values for a section of the winding

Turn	1	2	3	4	5
1	5.14e-07	3.75e-07	2.94e-07	2.38e-07	1.96e-07
2	3.75e-07	5.07e-07	3.76e-07	2.97e-07	2.42e-07
3	2.94e-07	3.76e-07	5.13e-07	3.83e-07	3.04e-07
4	2.38e-07	2.97e-07	3.83e-07	5.20e-07	3.90e-07
5	1.96e-07	2.42e-07	3.04e-07	3.90e-07	5.27e-07
6	1.64e-07	2.017e-07	2.49e-07	3.11e-07	3.97e-07
7	1.39e-07	1.69e-07	2.07e-07	2.55e-07	3.171e-07
8	1.19e-07	1.44e-07	1.75e-07	2.13e-07	2.60e-07
9	1.023e-07	1.23e-07	1.49e-07	1.80e-07	2.18e-07
10	8.82e-08	1.06e-07	1.279e-07	1.537e-07	1.84e-07

Table A. 2 Inductance values for a section of the winding

Appendix B: The Numerical Inverse Laplace Transform

The Laplace Transform is a very useful analysis tool. In this thesis the numerical inverse Laplace transform is applied to transform the transient response from frequency domain to time domain:

$$F(s) = \int_0^{\infty} f(t)e^{-st}\ dt \tag{A.1}$$

$$F(t) = (\frac{1}{2\pi j}) \int_{c-j\infty}^{c+j\infty} F(s)e^{st}\ ds \tag{A.2}$$

where $F(s)$ is a frequency domain signal, $F(t)$ is the corresponding time domain signal, s is the Laplace variable given by $s = c + j\omega$, where c is the real part (damping constant), and ω is the angular frequency. Alternatively, (A.1) and (A.2) can be expressed as:

$$F(s) = \int_0^{\infty} [f(t)e^{-ct}]\, e^{-jwt}\, dt \tag{A.3}$$

and

$$f(t) = (\frac{e^{ct}}{2\pi j}) \int_{-\infty}^{+\infty} F(s)e^{jwt}\ dw \tag{A.4}$$

From Eq. (A.3), it can be shown that the Laplace transform is equivalent to the Fourier transform of the damped signal $f(t)e^{-ct}$.

Gibbs oscillations errors can be introduced when using the numerical inversion of the Laplace transform. These errors are due to the truncation of the integration range. To overcome this problem a weighting function known as window is used. The Hanning window (σ) is used in this thesis:

$$\sigma = 0.5(1 + \cos(0.5\pi \frac{n+1}{N})) \tag{A.5}$$

Another type of error called aliasing can be introduced when using the numerical inverse Laplace transform; this is due to the discretization of the frequency error. This error can be reduced by applying the correct damping factor. The damping constant used in this thesis is given by [40]:

$$\mathrm{c} = 2\Delta\omega \tag{A.6}$$

The numerical evaluation described below is defined considering an odd sampling procedure in the frequency domain with spacing $2\Delta\omega$, and a conventional sampling in the time domain, where Δt represents the time step. The corresponding discrete functions in time and frequency domain are

$$f_n \equiv f(n\Delta t), \quad for\ n = 0,1,2, \ldots\ldots, N-1 \tag{A.7}$$

and

$$F_{2k+1} \equiv F(c + j(2k+1)\Delta\omega), \quad \text{for} \quad k = 0.1 \ldots\ldots\ldots, N-1 \tag{A.8}$$

where *N* is the number of discrete samples. Defining the observation time corresponding to the waveform period as

$$\Delta t = \frac{T}{N} \tag{A.9}$$

Considering an odd sampling and including the window function it follows that

$$f_n = \frac{e^{cn\Delta t}}{\pi}\ Re\left\{2\ \sum_{k=0}^{N-1} F_{2k+1}\ \sigma_{2k+1}\ e^{j(2k+1)n\Delta\omega\Delta t}\ \Delta w\right\} \tag{A.10}$$

Substitution Eq. (A.7) and Eq. (A.9) into Eq. (A.10) gives

$$f_n =\ Re\left\{C_n\ \sum_{k=0}^{N-1} F_{2k+1}\ \sigma_{2k+1}\ e^{j2\pi kn/N}\right\} \tag{A.11}$$

where

$$C_n = 2Ne^{cn\Delta t}\ e^{j\pi n/N}\ \Delta\omega/\pi \tag{A.12}$$

The numerical form of equation (A.11) allows using the Fast Fourier Transform (FFT) for computer time savings [40].